Available online at www.sciencedirect.com

SCIENCE DIRECT

Biochimica et Biophysica Acta 1707 (2005) 67–90

BIOCHIMICA ET BIOPHYSICA ACTA
BBA

http://www.elsevier.com/locate/bba

Review

Structure and interactions of amino acid radicals in class I ribonucleotide reductase studied by ENDOR and high-field EPR spectroscopy

Friedhelm Lendzian*

Max-Volmer-Laboratory for Biophysical Chemistry, Institute for Chemistry, PC 14, Technical University Berlin, Strasse des 17. Juni 135, D-10623 Berlin, Germany

Received 27 May 2003; accepted 17 February 2004
Available online 8 May 2004

Abstract

This short review compiles high-field electron paramagnetic resonance (EPR) and electron nuclear double resonance (ENDOR) studies on different intermediate amino acid radicals, which emerge in wild-type and mutant class I ribonucleotide reductase (RNR) both in the reaction of protein subunit R2 with molecular oxygen, which generates the essential tyrosyl radical, and in the catalytic reaction, which involves a radical transfer between subunits R2 and R1. Recent examples are presented, how different amino acid radicals (tyrosyl, tryptophan, and different cysteine-based radicals) were identified, assigned to a specific residue, and their interactions, in particular hydrogen bonding, were investigated using high-field EPR and ENDOR spectroscopy. Thereby, unexpected diiron-radical centers, which emerge in mutants of R2 with changed iron coordination, and an important catalytic cysteine-based intermediate in the substrate turnover reaction in R1 were identified and characterized. Experiments on the essential tyrosyl radical in R2 single crystals revealed the so far unknown conformational changes induced by formation of the radical. Interesting structural differences between the tyrosyl radicals of class Ia and Ib enzymes were revealed. Recently accurate distances between the tyrosyl radicals in the protein dimer R2 could be determined using pulsed electron–electron double resonance (PELDOR), providing a new tool for docking studies of protein subunits. These studies show that high-field EPR and ENDOR are important tools for the identification and investigation of radical intermediates, which contributed significantly to the current understanding of the reaction mechanism of class I RNR.
© 2004 Elsevier B.V. All rights reserved.

Keywords: Ribonucleotide reductase; High-field EPR; ENDOR; Tyrosyl; Tryptophan; Cysteine radical

1. Introduction

Ribonucleotide reductase (RNR) is a long known and probably the best-investigated radical enzyme. It catalyses the reduction of ribonucleotides to deoxyribonucleotides (Fig. 1), which is the rate-limiting step of DNA synthesis [1–5]. Therefore, RNR is an important target for cell growth control, and several RNR inhibitors are being used, or have been proposed, as drugs for chemotherapeutic treatment of cancer and virus infections based on radical scavenging, substrate analogues, or on peptidomimetic inhibitors [4–8]. Three main classes of RNRs have been described, classified according to the radical generator driving the catalytic reaction [4,8–13]. Class I enzymes produce a stable tyrosyl radical on one protein subunit in a reaction of a dinuclear iron center with molecular oxygen [1–5]. The Class II enzymes use the cofactor cobalamin for radical generation [4,12–14]. A thiyl radical, strongly coupled to the cobalt ion of the cobalamin, was reported to be the active radical, which drives substrate turnover in class II RNR [12,13]. Class III enzymes are strictly anaerobic and form a stable glycyl radical with the help of an iron–sulfur protein and *S*-adenosyl methionine [9–11,15]. Two landmarks for the

Abbreviations: EPR, electron paramagnetic resonance; ENDOR, electron nuclear double resonance; RNR, ribonucleotide reductase; R2, subunit of class I RNR, which carries the diiron site and the active tyrosyl radical; R1, subunit of class I RNR, which binds the substrate; hf, hyperfine; g, electronic g-tensor with principal values g_x, g_y, and g_z; Y122$^\bullet$, Y177$^\bullet$, W111$^\bullet$, W177$^\bullet$, tyrosyl and tryptophan radicals in wild-type and mutant R2 of *E. coli* and mouse

* Tel.: +49-30-314-22489; fax: +49-30-314-21122.
E-mail address: f.lendzian@tu-berlin.de (F. Lendzian).

0005-2728/$ - see front matter © 2004 Elsevier B.V. All rights reserved.
doi:10.1016/j.bbabio.2004.02.011

investigation of the last two classes were the X-ray structure analysis for the anaerobic class III enzyme in 1999 by Logan et al. [15] and recently, in 2002, also for the class II enzyme by Sintchak et al. [14].

Class I enzymes are found in practically all eukaryotic organisms, from yeast and algae to plants and mammals, and some prokaryotes and viruses also express this type. Class I RNR of *E. coli* was mostly used for studying structure/function or/reactivity relationship by investigating the wild-type and various mutants (for reviews, see Refs. [1–5,8]). It consists of two homodimeric proteins, R1 and R2, see Fig. 1 [1–5]. While the substrate turnover reaction is performed in R1, the role of protein R2 is to harbor in the active state a tyrosyl radical, Y122$^{\bullet}$ (*E. coli* numbering), which is needed for starting the catalytic reaction in R1 (see Fig. 1). The tyrosyl radical is located close to a diferric iron center, which couples antiferromagnetically to form an $S=0$ ground state. The X-ray structures have been determined separately for R2 [16] and also for R1 with substrate and one affector bound [17], see Fig. 1.

Catalytic models have been proposed based on these structural data. Catalytic activity requires a holoenzyme complex R1–R2, the structure of which is yet not known in detail. The catalytic reaction in R1 is believed to involve a coupled electron/proton (H$^{\bullet}$ radical) transfer via a conserved hydrogen-bonded pathway from the tyrosyl radical Y122$^{\bullet}$ in protein R2 to cysteine C439 in R1 (*E. coli* numbering). In R2, the pathway is made up of the iron ligands D84 and H118, and continues via D237 and W48, which is located close to the protein surface. In R1, two tyrosines Y730 and Y731 and cysteine C439, which is at the substrate binding site, are involved in the pathway, see Fig. 2 and Refs. [1–5,8,18–21]. The substrate turnover reaction in R1 is proposed to be initiated by a thiyl radical on C439

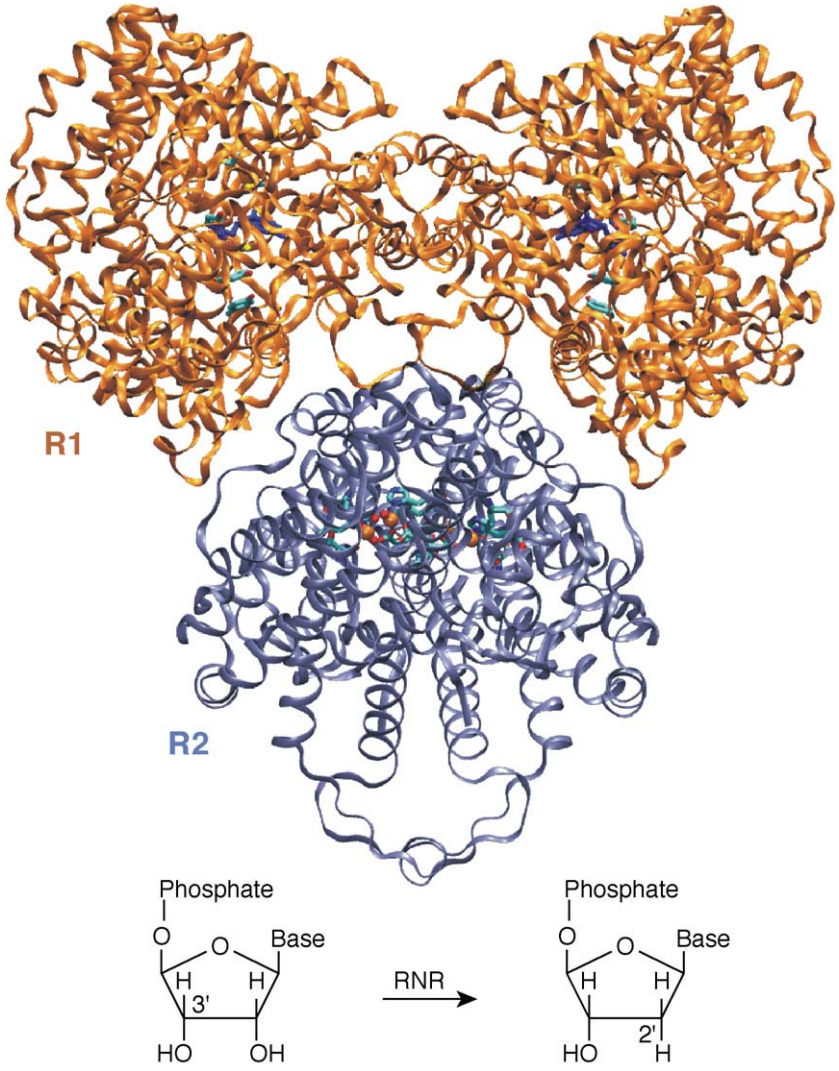

Fig. 1. X-ray structure of ribonucleotide reductase subunits R1 (gold) with bound substrate GDP and oxidized met R2 (blue) from *E. coli* [16,17,49]. The two Fe^{III} (yellow) with bridging oxygen and terminal water ligands (red), histidine ligands, and the tyrosine Y122 (cyan) in R2 and GDP (blue) in R1 are indicated. Relative arrangement of both subunits in analogy to Sjöberg [1]. Bottom: Reduction of a nucleotide to a deoxynucleotide.

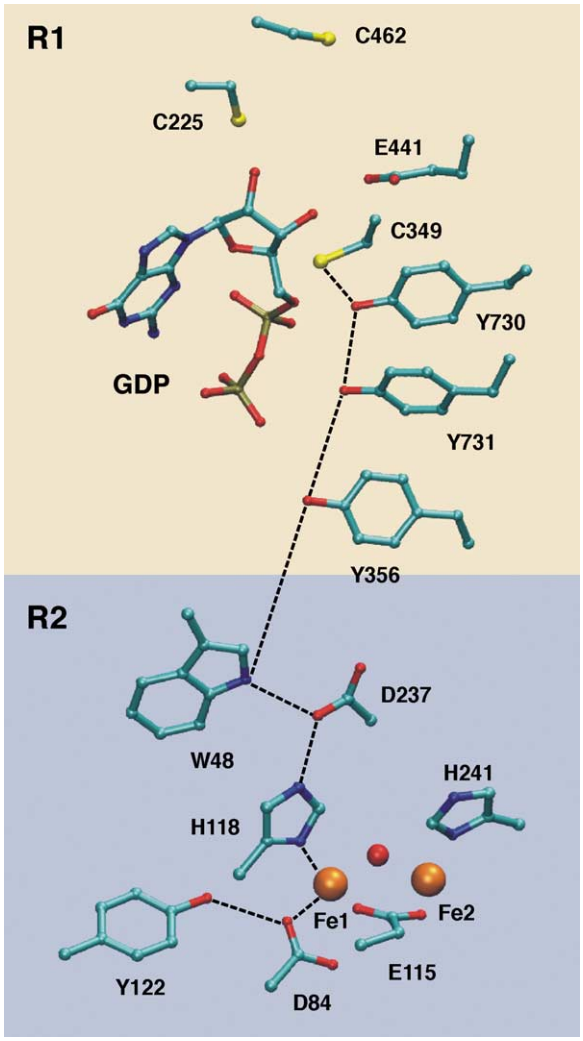

Fig. 2. Structure of the diiron site with tyrosine Y122 in RNR subunit R2 [16,49] (blue) of *E. coli*, and of the substrate binding site in subunit R1 [17] (gold) with bound substrate guanine diphosphate (GDP). The dashed line indicates the proposed reversible electron/proton (H$^{\bullet}$) transfer pathway along a network of conserved and hydrogen-bonded amino acid residues, which connect the diiron site in R2 with C439 at the substrate binding site in R1; see text and Refs. [1–5,8].

[3–5,8,19,21], which is generated in a radical transfer reaction from Y122$^{\bullet}$ in R2, which thereby transiently transfers its radical character to C439 and becomes reduced to Y122-OH. The putative thiyl radical C439$^{\bullet}$ then abstracts a hydrogen atom from the substrate [3,4,8,19]. In the course of the substrate turnover, a disulfide bridge is formed between C225 and C462 at the active site in R1 (Fig. 2) that must be reduced before a new substrate can bind. This is accomplished by the hydrogen donor proteins, thioredoxin or glutaredoxin, via a second disulfide bridge located on the surface of R1 [1–5,8,21]. After formation of the product (deoxyribonucleotide) and its release from R1, the radical transfer reaction is proposed to perform in the opposite direction, thereby restoring the initial tyrosyl radical Y122$^{\bullet}$ in R2 [1–5,8].

In class I RNR, so far, no intermediate amino acid radicals have been observed during the catalytic reaction in the wild-type enzyme along the proposed pathway (Fig. 2). Neither was the proposed thiyl radical at C439 directly observed. The involvement of this thiyl radical was, however, based on strong indirect evidence: In class II RNR a thiyl radical, coupled to cobalamin, close to the substrate has been observed [12,13]. Studies on class I RNR, using mechanism-based inhibitors, which substituted the substrate, showed that inhibitor radicals were generated in subunit R1 at the expense of the tyrosyl radical in subunit R2, in accordance with a reaction scheme assuming a thiyl radical at C439 [1,8]. Mechanistic models for the observed electron/proton (radical) transfer between R2 and R1 have been proposed [1–5,8,20]. The role of protein fluctuations involving simultaneous switching of several hydrogen bonds was emphasized to explain the experimental findings in wild-type and mutant RNR of *E. coli* [22,23]. More rigorous density functional theory (DFT) calculations have been performed for characterizing individual steps of the proposed electron/proton transfer reaction along the hydrogen-bonded amino acid chain [20].

The tyrosyl radical in subunit R2 is generated via the reductive cleavage of molecular oxygen at the diiron center either from reacting the apoprotein with Fe^{II} solution and molecular oxygen (reconstitution), or from reacting the diferrous R2 with molecular oxygen [5,24–26]. In the course of this reaction, a high-valent $Fe^{III}Fe^{IV}$ intermediate "X" [27,28] is formed, probably via a peroxo-diiron intermediate [29], which finally oxidises tyrosine Y122 to the radical form Y122$^{\bullet}$, turning the diiron cluster into the antiferromagnetically coupled diferric state [25–30]. The oxygen molecule is split, one oxygen is found as μ-oxo-bridge between the two irons [1]. Different amino acid radicals and diiron states, which emerge as intermediates during this reaction, have been studied in wild-type R2 and in a variety of mutants [31–36]. The iron-oxygen reconstitution reaction requires an extra electron [1,5,26,35–37], which comes from an external source, and it has been proposed that this electron transfer pathway in R2 could be similar to that for the catalytic transfer reaction between Y122$^{\bullet}$ in R2 and C439 in R1 [31,35–38].

Radicals are involved in the three reactions of class I RNR: (i) during the generation of the essential tyrosyl radical in a reaction of the diferrous iron center with molecular oxygen [1,26,31–38], (ii) in the radical transfer reaction [1–5,35,36] from the tyrosyl radical Y122$^{\bullet}$ in R2 to the putative thiyl radical in R1, which is prerequisite for staring substrate turnover [1,4,5,8,20], and (iii) in the catalytic cycle of substrate turnover, which is started by the putative thiyl radical at C439, and where intermediate radicals of substrate or substrate analogues and amino acid based radicals have been observed [3,8,39,40].

In all these reactions, identification and characterization of the structure and interactions of radicals, which emerge as intermediates in wild-type and in mutants of RNR, is of

key importance for understanding the mechanism. High-field electron paramagnetic resonance (EPR) and electron nuclear double resonance (ENDOR) spectroscopy have proven to be powerful tools for the investigation of protein-based radicals [40–48]. There are several reviews on the structure and function of RNR from the three classes [1–5,8]. The present paper gives a brief summary focusing on the different amino acid radicals, which emerge in wild type and mutants of class I RNR. Selected examples are presented to show how amino acid radicals can be identified, and assigned to specific residues, and their structure and interaction (e.g. hydrogen bonds) with the protein environment can be investigated by ENDOR and high-field EPR spectroscopy on frozen protein solutions. Furthermore, high-field EPR experiments on RNR single crystals [49] yield information on the structure and orientation of the tyrosyl radical in the active enzyme, so far not available from X-ray crystallography.

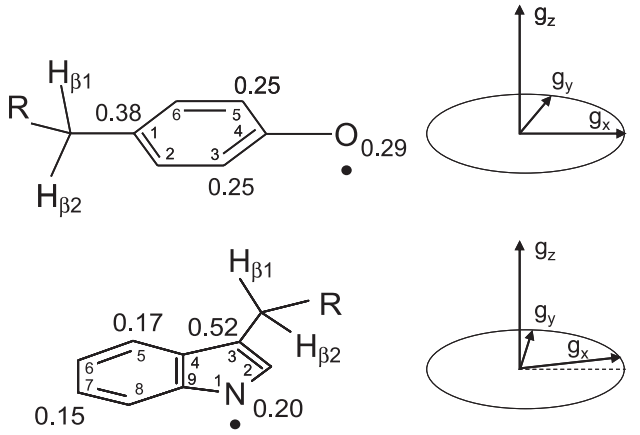

Fig. 3. Molecular structures of the tyrosyl (top) and tryptophan (bottom) radicals with numbering schemes. The large outer numbers are the p_z-spin densities at the respective carbon, oxygen and nitrogen nuclei, deduced from the experimental hyperfine coupling tensors (see text). The orientations of the *g*-tensor axes (right) coincide with the molecular axes for the tyrosyl radical [53]. For the tryptophan radical, the g_x-axis forms an angle of $\approx 20°$ with the molecular *x*-axis, as indicated [44].

2. Molecular parameters measured by EPR and ENDOR on radicals

EPR and ENDOR spectroscopy deliver information on the electronic structure of a radical, in particular on its *g*-factor and the hyperfine interactions between the unpaired electron and the magnetic nuclei of the radical [50–57]. The experimental spectra are interpreted based on the spin Hamilton operator

$$\mathscr{H} = \mu S\mathbf{g}B + \sum_k (\mu_{Nk} I_k g_{Nk} B + S\mathbf{A}_k I_k + I_k \mathbf{Q}_k I_k) \qquad (1)$$

where μ and μ_{Nk} are the electron and nuclear magnetons, respectively, B is the applied magnetic field, and S and I are the respective electron and nuclear spin operators. **g** is the electronic *g*-tensor which is anisotropic with principle values g_x, g_y, and g_z, and which results from spin-orbit coupling of the unpaired electron in the radical. Therefore, these *g*-tensor values are a fingerprint for the respective type of radical (see below). The orientation of the *g*-tensor principle axes, *x*, *y*, and *z* reflects the orbital symmetry of the radical. For a tyrosyl radical, these have been determined from experiments on irradiated tyrosine single crystals [53] and are shown in Fig. 3. $\mathbf{A}_k$ are the hyperfine (hf) coupling tensors of the different magnetic nuclei k with nuclear spin $I>0$ in the radical, which have principal components A_{xk}, A_{yk}, A_{zk}. The orientations of their principle axes are often collinear with local bond axes and do in general not coincide with the principle axes of the *g*-tensor. The isotropic part of a particular hyperfine tensor ($A_{isok}=(A_{xk}+A_{yk}+A_{zk})/3$) reflects the unpaired electron spin density in the s-orbital of the respective nucleus, from which the spin density in the p_z-orbital of nucleus k or, in case of hydrogen nuclei, the p_z-orbital of the neighboring carbon or nitrogen nucleus in the radical can be deduced [54,55,57]. Evaluation and assignment of all observed hf-tensors reveals in detail the distribution of the unpaired electron in the radical [50–53]. For nuclei with spin $I\geq 1$ (e.g. ^{14}N with nuclear spin $I=1$) the nuclear quadrupole coupling tensor, $\mathbf{Q}_k$, has to be considered [56,57], which results from interaction of the nuclear electric quadrupole moment with the electric field gradient tensor at the nucleus, generated by the charge distribution of all electrons.

Most EPR and ENDOR experiments are performed on frozen protein solutions or single crystals at low temperatures. Therefore, the anisotropy of the above mentioned interactions is observed in the spectra. It should be noticed however, that at least for larger proteins (molecular weight larger than 10 000 Da) the time scale of rotation in liquid solution is slow compared with the frequency scale of hyperfine interactions and *g*-anisotropy, so that "immobilized spectra" are expected also from liquid protein solutions. The observed EPR spectrum of a protein-based radical is therefore the superposition of spectra from all different orientations of the radical with respect to the orientation of the external magnetic field. Thereby the *g*-tensor gives rise to orientation-dependent resonance positions (in analogy to the chemical shift tensor in NMR), whereas the hf-tensors $\mathbf{A}_k$ lead to orientation-dependent splitting in the spectrum. The quadrupole interaction is in first order not observed in EPR, but is observed in ENDOR for all nuclei with spin $I\geq 1$. At conventional EPR frequency (9.5 GHz corresponding to a field of 0.34 T), the effects of *g*-anisotropy and hyperfine splitting in the spectra are often of the same order of magnitude, and consequently not all parameters can be obtained from the EPR spectrum. In these cases, it is advantageous to apply high-frequency/high-field EPR (e.g. 94 GHz, corresponding to a field of 3.35 T) to separate the *g*-components in the spectra thereby increasing the spectral resolution.

An alternative technique to improve spectral resolution is ENDOR. In this technique, the intensity of an EPR signal is monitored as function of an irradiated frequency in the range of nuclear spin transitions (NMR), thereby enabling to obtain the NMR spectrum of the paramagnetic species with good spectral hyperfine resolution even in cases of poorly resolved EPR spectra [48,50–57]. At conventional 9.5-GHz EPR frequency, usually all orientations of a radical species contribute to the ENDOR spectrum recorded for the center of the EPR spectrum, which leads to a "powder pattern" line shape for all ENDOR transitions. In this case for ^{1}H (I = 1/2) nuclei, pairs of spectral features (turning points or peaks in absorption mode, peaks and zero crossings in derivative mode) are observed for each of the three principal components A_j ($j = x, y, z$) of a hyperfine tensor according to the first order ENDOR resonance condition

$$\nu_{\pm}(\mathrm{ENDOR})_j = |\nu_N \pm (A_j/2)| \quad (2)$$

and the full hyperfine (hf) tensors can be obtained from the ENDOR spectra. The spectral lines are in first order spaced symmetrically around the nuclear Zeeman frequency ν_N (for 9.5-GHz EPR, this is 14.4 MHz for ^{1}H) in case of $\nu_N > |A_j/2|$, or around the respective hyperfine value $A_j/2$, in case of $\nu_N < |A_j/2|$ [28,50,57]. For nuclei with spin $I \geq 1$, the quadrupole interaction $I_k \mathbf{Q}_k I_k$ in Eq. (1) leads to an additional splitting in the ENDOR spectra. For ^{14}N with nuclear spin $I = 1$, an additional term of $\pm 3Q_j/2$ is obtained for the ENDOR resonance condition, Eq. (2), where Q_j is the value of the quadrupole tensor $\mathbf{Q}$ for the respective axis ($j = x$, y, or z) [56,57]. These first order terms are usually appropriate for the case of free radicals. However, spectra recorded at low fields may require second order corrections [57]. Additional terms describing spin coupling may be required for Eq. (1) in case of radicals interacting with a metal center [13].

Particularly useful is the combination of high-field EPR with ENDOR. At high magnetic field, the g-tensor components are well separated in the EPR spectra, and ENDOR spectra recorded for the outermost low-field and high-field EPR positions correspond to the x- and z-orientations of the g-tensor. In this way, ENDOR spectra are obtained, which correspond to certain molecular orientations, even from solution samples, and relative orientations of g- and hf-tensor axes can be obtained with good accuracy. This technique has been applied to the tyrosyl radical in class I RNR from *E. coli* and yeast [45,47,48].

Angular dependent high field EPR spectra recorded from protein single crystals, which are rotated in the external field, enable not only the determination of tensor principal values, but also the determination of g- and hyperfine tensor axes orientations for a radical with respect to the crystal symmetry axes. This has been achieved for the RNR R2 protein of *E. coli* in one study, revealing the amount of reorientation of the tyrosyl radical as compared with the X-ray structure of the protein with the normal reduced tyrosine [49].

The above mentioned EPR and ENDOR techniques can be applied in continuous wave (cw) mode, when usually first derivative mode spectra are recorded. In many cases, pulsed EPR and ENDOR techniques are experimentally advantageous, where the intensity of a spin echo signal is monitored leading to absorption mode spectra. Both techniques yield essentially the same spectral information on g- and hyperfine tensors. Pulse EPR techniques require, however, microwave pulses, which are short compared with the spin relaxation times of the investigated radical, T_1 (longitudinal) and T_2 (perpendicular). In a simple two pulse spin echo experiment, a first short microwave pulse (90° pulse) generates magnetization perpendicular to the magnetic field, which decays due to phase decoherence with time constant T_2. After time τ, a short second pulse (180° pulse) is applied, which refocuses the magnetization, leading to a short strong spin echo signal at time τ after the refocusing pulse. Spectra may be obtained by recording the echo signal intensity as function of the magnetic field. The intensity of the echo signal decays due to spin relaxation during the time interval between the first pulse and the echo (2τ) with the time constant T_2. This offers an elegant method to discriminate between signals from two species having different T_2 values by using appropriate τ values (see below). A variety of advanced pulse EPR and ENDOR techniques has been developed, some of them using one or two dimensional Fourier transformation of the recorded modulated time traces. A detailed description of pulse-EPR and ENDOR techniques is beyond the scope of this article and the reader is referred to Refs. [58–61].

A new and promising pulse EPR technique, pulsed electron–electron double resonance (PELDOR), shall be mentioned, which enables determination of small dipolar interactions between two radical species, from which the accurate distance between the two species can be obtained. This can provide important information, e.g. on docking of protein subunits, which cannot be co-crystallized. For this technique, the reader is referred to Refs. [61,62].

3. The tyrosyl radical in class I wild-type RNR

The tyrosyl radical Y122• (Fig. 3) in class Ia RNR of *E. coli* was first detected by EPR by Ehrenberg and Reichard in 1972 [63] and unambiguously identified as tyrosyl radical by Sjöberg et al. [64] using selective isotope labeling of the tyrosines in the enzyme.

3.1. Hyperfine structure of tyrosyl radicals in RNR

The hyperfine structure of the tyrosyl radical Y122• in R2 of *E. coli* has been characterized in detail by ENDOR [47,51,52]. 9.5 GHz-ENDOR spectroscopy was first applied on Y122• in RNR of *E. coli* by Bender et al. [52] and Hoganson et al. [51] to obtain the hf tensors from the tyrosyl

ring protons and the β-protons of the side chain (Fig. 3). An extensive 140-GHz ENDOR study on Y122• has been performed more recently, yielding the relative orientations of *g*- and hyperfine tensors, and accurate values for the small hf-tensors of the ring protons at positions 2 and 6 and for the small hf-tensor of the second β-proton of the side chain [48]. These studies yielded a detailed picture of the spin density distribution of this tyrosyl radical. Fig. 3 shows the molecular structure and the major spin densities [51] deduced from ENDOR on Y122• of *E. coli*. The measured hf-tensor components are collected in Table 1.

Tyrosyl radicals have been studied also from class I RNR of other organisms. ENDOR studies have been performed at 35 GHz on Y177• of the mouse enzyme [65]. In recent years the structure and function of yeast RNR have been investigated, which exhibits a heterodimeric Y2Y4 protein structure [45,66,67]. Its tyrosyl radical has been extensively investigated by ENDOR performed at 140-GHz EPR frequency [45]. For both radicals, the relative orientation of the axes of the *g*- and hf tensors was obtained. A particular important finding was in both these enzymes from mouse and yeast, the presence of a hydrogen bond to the tyrosyl C=O group, as proven by ^{2}H-ENDOR on samples exchanged in ^2H_2O [45,65]. This was in contrast to the tyrosyl radical in *E. coli*, which is not hydrogen-bonded (Refs.[45,65], see below).

Furthermore, tyrosyl radicals in RNR of plants [68,69] and of a variety of microorganisms and also viruses have been studied [65,70–76]. Of particular interest was the observation of different hyperfine values, $A_{iso}(H_{\beta 1,2})$, for the side chain β-protons of the tyrosyl radicals from different organisms (Table 1). Three groups of tyrosyl radicals were observed. One group of radicals, e.g. in *E. coli* [51,52] and yeast [45], exhibited only one large hyperfine coupling of approximately 2.0 mT from one β-proton of the side chain. Another group of radicals, e.g. in mouse, *Herpes simplex virus* (HSV1) [65], and *Arabidopsis thaliana* [68,69] exhibited one large, and one small hyperfine coupling (1.8–2.0 mT, and 0.6–0.7 mT) from both of the β-protons of the side chain. A third group of tyrosyl radicals, e.g. in *Mycobacterium tuberculosis* [72], *Salmonella typhimurium* [73], and *Corynebacterium ammoniagenes* [74], exhibits only one small β-proton hyperfine coupling of 0.8–0.9 mT (see Table 1).

The first two of these groups belong to class Ia enzymes, which are found in mammals, plants, yeast, DNA viruses and in *E. coli*; the third group belongs to class Ib enzymes, which are found only in prokaryotic organisms and which differ also in their pattern of allosteric regulation [77].

It was found that the overall spin density distributions of the tyrosyl radicals from all three groups in both classes Ia and Ib were very similar [51,72]. The large difference of the hyperfine couplings of the β-protons was instead attributed to a different geometry of the tyrosyl side chains (Ref. [51], see Fig. 3). The isotropic part A_{iso} of the hyperfine coupling of a β-proton does not only depend on the spin density of the adjacent carbon of the ring system (C1, see Fig. 3, and chapter 2), but, in addition, there is a strong dependence on the geometry of the side chain according to

$$A_{iso}(H_{\beta 1,2}) = \rho^{\pi}_{C1}[B' + B''\cos^2(\theta)] \quad (3)$$

where ρ^{π}_{C1} is the π-spin density at carbon C1, and θ is the dihedral angle between the respective β-proton and the p_z-

Table 1
Hf tensor principal values [mT] of tyrosyl radicals in class I RNR from selected organisms

Tyrosyl radical, organism	A_x (3,5)[a]	A_y (3,5)[a]	A_z (3,5)[b]	$A_{iso}(H_{\beta 1})$[c]	$A_{iso}(H_{\beta 2})$
Y•, *E. coli* [51][d]	−0.95	−0.30	−0.70	2.01[e]	−0.01
Y•, *E. coli* [48][d]	−0.94	−0.29	−0.69	1.97[e]	0.04
Y•, *E. coli* [44][d]	−0.96	−0.28	−0.70	2.06[e]	<0.2
Y•, yeast [45][d]	−1.00	−0.40	−0.60	2.12[e]	0.29
Y•, mouse [44][d]	−0.91	−0.44	−0.66	2.06[e]	0.59
	−0.75	−0.49	−0.58		
Y•, mouse [71][d]	−0.91	−0.44	−0.66	2.06[e]	0.59
	−0.73	−0.48	−0.58		
Y•, *Arabidopsis thaliana* [68,69][d]	n.g.[f]	n.g.[f]	n.g.[f]	1.80[e]	0.7
Y•, *Mycobacterium Tuberculosis* [72][g]	−1.17	−0.19	−0.71	0.84[e]	0.2
Y•, *Salmonella thyphimurium* [73][g]	−1.15	−0.25	−0.71	0.91[e]	<0.3

[a] The hyperfine tensor principal axes *x* and *y* for the protons at positions 3 and 5 (Fig. 3) are rotated by approximately +25° (position 3) and −25° (position 5) with respect to the *g*-tensor *x*- and *y*-axes [44,45,47,51,73]. Hyperfine tensor components $A_{x,y,z}$ for positions 2 and 6 are approximately 0.18, 0.27, and 0.08 mT for all tyrosyls [45,48,51] and correspond to a small negative spin density of −0.08 at carbons 2 and 6 [51]. 1 mT=28.0 MHz.

[b] *z*-axes of hyperfine tensors of position 3 and 5 and *g*-tensor *z*-axis are collinear (see Fig. 3).

[c] Isotropic values $A_{iso}=1/3(A_x+A_y+A_z)$.

[d] Class Ia RNR.

[e] Estimated dihedral angles θ from Eq. (3) using $\rho^{\pi}_{C1}=0.38-0.39$ and B″ ≈ 5.24–5.7 mT [51,78] are for the tyrosyl radicals in the class Ia enzymes of *E. coli*, and yeast: $\theta_1 \approx -10° - -20°$, $\theta_2 \approx +110° - +100°$; for mouse and *A. thaliana*, $\theta_1 \approx +10° - +20°$, $\theta_2 \approx +130° - +140°$; and for the radicals in the class Ib enzymes of *M. tuberculosis* and *S. thyphimurium*, $\theta_1 \approx -50°$, $\theta_2 \approx +70°$. Angles are defined with respect to the p_z axis, see Fig. 6B.

[f] Values not given in Refs. [68,69], but reported to be similar as for mouse [68,69].

[g] Class Ib RNR.

axis [51]. B′ and B″ are empirical constants, where B′ is usually assumed to be zero and B″ has a value of 5.24–5.7 mT [51,78]. Estimated side chain orientations, deduced from the experimental $A_{iso}(H_{\beta 1,2})$ values, are given in Table 1, caption. It has been proposed that different side chain orientations might effect the redox potential, thereby influencing the reactivity [79]. Theoretical studies [78] showed that the side chain geometries of the tyrosyl radicals Y122• in *E. coli* RNR and of the tyrosyl radical in class Ib RNR, which is very similar to the dark stable Y_D • in plant PSII [80], correspond to two energetic minima. However, there was a shallow broad energy minimum calculated for a large range of side chain orientations [78] similar to that of the class Ib tyrosyls, indicating that the actual side chain geometry for a given species seems largely determined by protein constraints.

It is interesting that in all class Ia RNR enzymes, the tyrosyl radicals exhibit similar side chain orientations (deviations are max. ±10°, see Table 1, caption), whereas in class Ib enzymes the tyrosyl side chain orientation is ≈ 40° different from that in *E. coli* and similar to that of the tyrosyl radical YD• in plant PS II [51,72,80]. It has been concluded from EPR experiments that in class Ib the tyrosyl radical is in a more rigid protein pocket [72] as compared with class Ia. Comparison of the X-ray structures showed that in class Ib RNR of *S. typhimurium* the site of the active tyrosine is 6.5–7.0 Å away from the diiron center, whereas this distance is only ≈ 5.0 Å in class Ia *E. coli* [16,75,76]. In class Ib there is a water molecule between the radical site and the aspartate ligand of Fe1, which is absent in class Ia [16,75,76]. This explains the different EPR relaxation behaviour found for class Ia and class Ib tyrosyl radicals [45,51,65,68–74]. Possible functional implications of this finding are still under debate [72–76].

3.2. g-tensor of tyrosyl radicals in RNR

The three principal components, g_x, g_y, g_z, of the *g*-tensor of the tyrosyl radical are only resolved in EPR spectra recorded at frequencies at least 10-fold higher than conventional X-band frequency (9.5 GHz). First accurate determination of the *g*-tensor for a tyrosyl was performed by Gerfen et al. [42] on Y122• of *E. coli* using 140-GHz high-field EPR spectroscopy.

Unlike the hyperfine couplings, which reflect the local spin densities at the respective nuclei, the *g*-tensor of an aromatic π-radical is an integral property of its wave function. Deviations of the principal values of the *g*-tensor from the free electron value ($g_e = 2.0023193$) result from spin orbit coupling, and are in π-radicals pronounced only for the in plane tensor components g_x and g_y, whereas the out-of-plane component g_z is close to the free electron value [81] (for axes, see Fig. 3). Since the spin orbit coupling constants, ξ, increase with the atomic weight ($\xi = 28$, 76, and 151 cm^{-1} for C, N, and O, respectively; Ref. [54]), the deviations from the g_e-value are in organic radicals particularly large when large spin densities occur on heavier atoms, like oxygen.

It was observed by several groups that the g_x component of tyrosyl radicals in class I RNR has not the same value for all organisms [41–45,65,70–74,82,83]. Table 2 summarizes *g*-tensor values for tyrosyl radicals from selected class Ia and Ib RNRs. It is obvious that there are two groups of tyrosyl radicals, one with g_x-values around 2.0076, another group with g_x-values around 2.0089–2.0092. Fig. 4 shows a comparison of the 94-GHz EPR spectra of the tyrosyl radical Y122• in *E. coli* with that of the respective analogue, Y177•, in the mouse enzyme (adopted from Ref. [83]). The g_x-value is shifted from a high value (≈ 2.0092) in *E. coli* to a significantly lower value (≈ 2.0076) in mouse (Table 2). It has been shown, both experimentally and theoretically, by several laboratories [41,44,45,65,70–73,82,84] that the value of the g_x-component of the tyrosyl radical is sensitive to electrostatic interactions and in particular to hydrogen bonds between the C=O group of the tyrosyl and the protein environment [43,44,48,65,70,82]. The different g_x-values indicate that Y122• in *E. coli* is located in a hydrophobic pocket and is not hydrogen-bonded, whereas Y177• in mouse exhibits a hydrogen bond at its carbonyl group [44,45,65,68]. The hydrogen bonds for Y177• in mouse and for the tyrosyl radical in yeast have been unambiguously confirmed by ^2H

Table 2
g-tensor principal values of tyrosyl and tryptophan radicals in class I RNR from selected organisms

Radical, organism (class)	g_x[a]	g_y[a]	g_z[a]	References
Y•, *E. coli* (Ia)	2.00912	2.00457	2.00225	[42,48]
Y•, *E. coli* (Ia)	2.00912	2.00454	2.00219	[49]
Y•, yeast (Ia)[b]	2.00770	2.00435	2.00229	[45]
Y•, mouse (Ia)[b]	2.0076	2.0043	2.0022	[65,71]
Y•, mouse (Ia)[b]	2.0076	2.0044	2.0021	[44]
Y•, *Herpes simplex virus* (HSV1) (Ia)[b]	2.0076	2.0043	2.0022	[65,71]
Y•, *Arabidopsis thaliana* (Ia)	2.0078	2.0043	2.0022	[68,69]
Y•, *Mycobacterium tuberculosis* (Ib)	2.0092	2.0046	2.0022	[70,72]
	2.0080			
Y•, *Salmonella Thyphimurium* (Ib)	2.0089	2.0043	2.0021	[73]
W111•, *E. coli* Y122F	2.0033[c]	2.0024	2.0021	[44]
W177•, mouse Y177W	2.0035[c]	2.0025	2.0023	[44]

[a] For the tyrosyl radicals, high g_x-values (≈ 2.0092) indicate a hydrophobic environment, low g_x-values (≈ 2.0076) indicate a hydrogen bond to the tyrosyl oxygen; see text [41–45,65,70–73,82]. The orientations of the corresponding tensor principal axes for the tyrosyl radical [53] are shown in Fig. 3.

[b] A hydrogen bond to the tyrosyl oxygen was verified by ^2H-ENDOR spectroscopy [45,65].

[c] Tryptophan neutral radicals, both hydrogen-bonded at the nitrogen [33,34]. The g_x-axis is rotated ≈ 20° with respect to the molecular *x*-axis [44], see Fig. 3.

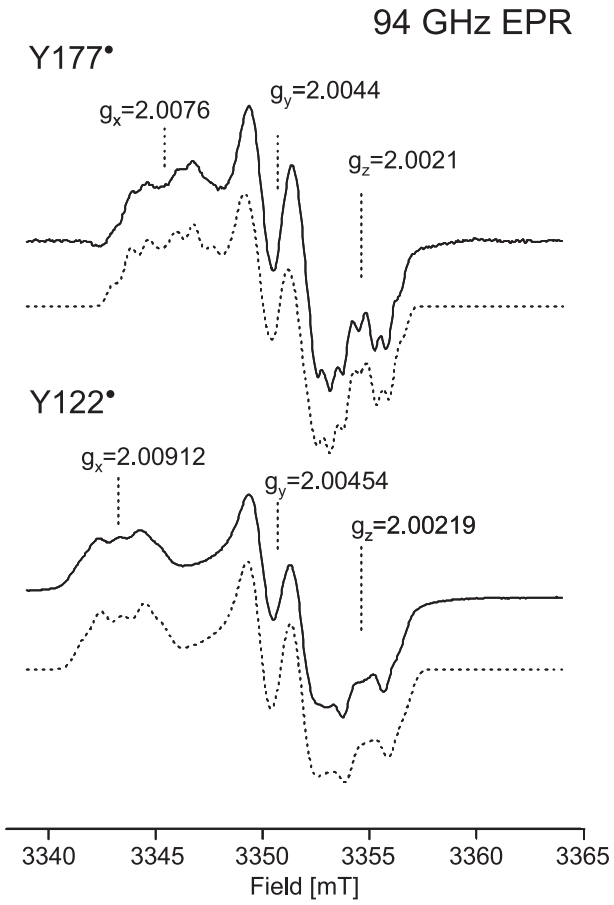

Fig. 4. 94-GHz EPR spectra of the catalytically active tyrosyl radicals Y122• in RNR subunit R2 of *E. coli* and Y177• in mouse RNR (adopted from Ref. [83]). Experimental conditions: microwave power (P_{mW}), 5 μW; modulation amplitude (ma), 0.4 mT; T=20 K. Dotted lines: simulated spectra using a program, described in Refs. [33,44]. The shift of the g_x-component in Y177• was attributed to a hydrogen bond; see text and Ref. [65].

ENDOR spectroscopy performed at 35 GHz [65] and at 140 GHz [45], respectively.

When comparing the g- and hyperfine values of the tyrosyl radicals in the different organisms depicted in Tables 1 and 2, there seems to be no obvious correlation between hydrogen bonding of the tyrosyl C=O group and the side chain orientation. The tyrosyl radicals of the class Ia enzymes of *E. coli* and yeast exhibit similar hf-tensor values and side chain orientations. Their g_x-values indicate, however, hydrogen bonding only for the radical in yeast. Apparently, both these features are independently imposed by the respective protein environment. These differences among the tyrosyl radicals of the various species, in particular the hydrogen bonding, are nevertheless expected to affect the reactivity, e.g. by changing the redox potential of the radicals. This may indicate a fine-tuning of the physico-chemical properties of these radicals in the different organisms.

The functional implications of the observed differences among the tyrosyl radicals are difficult to assess. A pathway of hydrogen bonds between amino acid residues in subunit R2, which is extending in R1 all the way to the substrate binding site (Fig. 2), was shown to be essential for enzyme function. Whenever this hydrogen bond pathway was interrupted by mutations, this resulted in a lack of catalytic activity [1–5,8]. Based on this experimental finding, functional models [1–5,18–20,22,23] were developed for class I RNR, where hydrogen bonds play a major role in the process of transferring the radical character from Y122• in R2 to C439 in R1. In this context, it is amazing, and until now not well understood, why the tyrosyl radical in some cases, like in *E. coli* and in *A. thaliana* RNR, is not hydrogen-bonded, whereas the tyrosyl radical in mouse, in *Herpes simplex*, and in yeast RNR is hydrogen-bonded [44,45,65,69]. It is noteworthy that the tyrosyl radical in class Ib *M. tuberculosis* was found to exhibit a heterogeneity showing two g_x-values, 2.0092 and 2.0080, or, in aged samples, a broad distribution between those values. It has been speculated that the enzyme may be activated by connecting the radical to the chain of hydrogen bonds [70].

Recently, a homologue of the small subunit of mammalian RNR, p53R2, was investigated, which was induced in response to DNA damage by the p53 protein [85]. It exhibits a stable tyrosyl radical, which has been investigated by 9.5-GHz EPR and showed similar hyperfine patterns as Y177• in class Ia mouse RNR [86]. It will be very interesting to further investigate this tyrosyl radical in p53R2 by high-field EPR and ENDOR. Possible differences of its structure and interactions with the protein environment might be related to the different function of p53R2 and its role in tumor suppression of p53 [85,86].

4. Radicals in the iron/oxygen reconstitution reaction in subunit R2

The radical Y122• (*E. coli* numbering) is generated from reacting either the apoprotein with Fe^{II}-solution and molecular oxygen (reconstitution), or from reacting the diferrous R2 with molecular oxygen [5,24,26,35]. The reaction proceeds according to [35]

$$\mathrm{Apo-R2-Y122} + 2\mathrm{Fe^{II}} + \mathrm{O_2} + \mathrm{H^+} + \mathrm{e^-} \Rightarrow \mathrm{R2-Y122^{\cdot}} + \mathrm{Fe^{III}-O-Fe^{III}} + \mathrm{H_2O}. \quad (4)$$

During the reaction, a high-valent diiron intermediate "X" is formed, probably from a peroxy precursor [29,35–37]. This intermediate "X" has been investigated in great detail by ENDOR at 35 GHz, and was characterized as a $Fe^{III}Fe^{IV}$ state [27,28]. This $Fe^{III}Fe^{IV}$ state has sufficient oxidation power to finally oxidize Y122 and generate the radical Y122•, thereby turning the diiron cluster into the antiferromagnetically coupled diferric state [30,35–37]. In the course of this reaction, the oxygen molecule is split and one oxygen atom forms a μ-oxo-bridge between the two

irons [1,34–36]. The reaction requires one proton and one extra electron, in addition to the three electrons from the two irons and the tyrosine [1–5,30,34–37]. It has been proposed that this electron could come from a reductant attached to the surface, and that thereby the same electron/proton transfer mechanism could be involved as for the catalytic radical transfer between Y122• in R2 and C439 in R1 [30,34–37]. A series of mutants has been investigated, where the active tyrosyl radical has been replaced by other amino acids in order to investigate the mechanism and intermediates of the iron/oxygen reconstitution reaction in RNR subunit R2 in more detail, and to explore which amino acid radicals other than tyrosine may be generated and may be possibly functional competent.

4.1. Tryptophan radicals in mutants of R2 of E. coli and of mouse

4.1.1. Hyperfine structure from ENDOR at 9.5 GHz

4.1.1.1. Y122F, E. coli. When tyrosine Y122 in R2 of *E. coli* was replaced against phenylalanine (Y122F), several radicals with different hyperfine structure have been observed as reaction intermediates of the iron/oxygen reconstitution reaction, Eq. (4) [32,33,44]. 9.5-GHz EPR spectra have been obtained from radicals both in room temperature stopped flow EPR experiments [32] and from samples freeze-quenched after ≲30 s to 77 K and measured at 77 K [32] or 10 K [32,33]. Two of the observed radicals, one measured in stopped flow room temperature EPR, the other measured in freeze-quenched samples at 77 K, were identified as tryptophan radicals based on isotopic labeling using indole-d_5 tryptophan [32,33]. EPR and 9.5-GHz ENDOR experiments performed at 10 K yielded a detailed picture of the spin density distribution of the tryptophan radical observed in the freeze-quenched samples. Hyperfine (hf) tensors were obtained from simulations of the EPR spectra and from ENDOR [33] for the ^{14}N nucleus, two ring ^{1}H nuclei (protons) and for the β-protons of the side chain attached at position C3 (for structure, see Fig. 3). Very similar hf tensor values for the two ring protons and for ^{14}N1 were obtained for the second tryptophan radical observed in the room temperature stopped flow spectra [33]. An assignment of the ring protons to positions 5 and 7 (Fig. 3) was based on isotopic labeling experiments and on DFT calculations [33]. The obtained hyperfine data are collected in Table 3; the derived π-spin densities are indicated in Fig. 3.

Oxidized tryptophan radicals may occur as cation radicals or, when deprotonated at N1, as neutral radicals (see Fig. 3). A tryptophan cation radical has been observed as a catalytic intermediate in cytochrome *c* peroxidase [56]. Besides tyrosyl radicals [87,88], a chain of tryptophan cation radical intermediates has been observed in the electron transfer process in DNA photolyase, whereby the last radical was transformed to a tryptophan neutral radical [87,89]. Based on comparison of the observed hf tensors with the results from density functional calculations performed for the tryptophan cation and for the neutral radical, both observed radicals in the R2 mutant Y122F of *E. coli* were assigned to the tryptophan neutral radical form, i.e. deprotonated at the nitrogen. The assignment to a neutral radical was further corroborated by the observation of a small ^{1}H-hf-tensor by ENDOR, which agreed in all three components with those calculated for a proton hydrogen-bonded to N1 [33]. These radicals in mutant Y122F of *E. coli* were rare examples for tryptophan neutral free radicals, which could be fully characterized by EPR and ENDOR in an enzyme, and which were not affected by magnetic coupling to a metal center. An earlier reported tryptophan cation radical in cytochrome *c* peroxidase [56] showed a coupling to the heme iron, which significantly changed its *g*- and hyperfine pattern. Another example of a freeze-quenched tryptophan free radical has been found recently in catalase peroxidase and characterized by high-field EPR [90].

The hf data from the β-protons of the side chain of the observed tryptophan radicals in mutant Y122F were of particular interest. Two large β-proton hyperfine couplings were observed for the freeze-quenched tryptophan radical in mutant Y122F R2 (Table 3). Since these couplings are strongly dependent on the dihedral angle of the respective

Table 3
Hf tensor principal values [mT] of tryptophan radicals in mutants of class Ia RNR

Tryptophan radical, organism	Tensor element	A_i (^{14}N)[a]	A_i (β_1)[b]	$A_i(\beta_2)$[b]	A_i(H5)[c]	A_i(H7)[c]	A_i(HB)[d]
W111• *E. coli* Y122 F [33]	*x*	≥ 0.10	1.36(2)	2.83(2)	− 0.63(2)	≥ |0.15|	− 0.118(5)
	y	≥ 0.10	1.36(2)	2.83(2)	≥ |0.15|	− 0.56(2)	0.193(5)
	z	1.05(2)	1.36(2)	2.83(2)	− 0.52(2)	− 0.46(2)	− 0.079(5)
W177• mouse Y177W [34]	*x*	≥ 0.07	2.25(2)	0.15(2)	− 0.65(2)	≥ |0.14|	− 0.12(1)
	y	≥ 0.07	2.25(2)	0.15(2)	≥ |0.14|	− 0.65(2)	0.18(1)
	z	0.94(2)	2.25(2)	0.15(2)	− 0.49(2)	− 0.49(2)	− 0.06(1)

[a] Orientation of the hyperfine tensor principal axis *z* is perpendicular to the molecular plane; see Fig. 3. 1 mT = 28.0 MHz.
[b] Side chain orientations calculated based on Eq. (2) are shown in Fig. 6.
[c] Orientation of the principle axis x of the hf-tensor for H(5) deviates 10° from molecular *x*-axis; principle axis *y* of the hf-tensor for H(7) deviates 30° from molecular *y*-axis [44], see Fig. 3.
[d] Hyperfine tensor from a proton hydrogen-bonded to N1, determined by H_2O/D_2O exchange experiments [33,34].

β-proton (Eq. (3)), both the spin density at carbon position 3 (Fig. 3) and the side chain orientation were obtained from the two observed β-proton hyperfine couplings [32,33]. Comparison of the side chain orientation obtained from EPR with the X-ray structures of the respective native proteins enabled an assignment of this tryptophan radical to residue W111. The second tryptophan radical observed in the room temperature stopped flow EPR experiments exhibited only one β-proton hyperfine coupling and was assigned in the same way to residue W107 [32,33]. The distance to the iron site (tryptophan edge to Fe2) was ≈ 4 Å for W111 and ≈ 8 Å for W107 [16]. This spectroscopic assignment to a specific tryptophan residue provided an interesting noninvasive alternative for site-directed mutagenesis.

The generation of transient tryptophan radicals on residue W111 and subsequently on residue W107 and the involved electron and proton pathways were further explored by a comparative investigation of the iron/oxygen reconstitution reaction of Y122F and of the double mutant Y122F/W107Y. For the double mutant, formation of a tyrosyl radical at Y107 was observed with a rate constant similar to that for formation of W111• in mutant Y122F. This indicated that the radical transfer between W111• and Y107 was very efficient in the double mutant and, consequently, the tryptophan radical W111• became very short-lived [91].

4.1.1.2. Y177W, mouse. A short-lived tryptophan radical was also observed for mutant Y177W of the mouse RNR, when the iron/oxygen reconstitution reaction was freeze-quenched after ≈ 30 s [34]. This mutant was of particular interest, since the catalytic essential tyrosine Y177 was directly replaced by tryptophan. Again, the radical was identified using samples with isotopic labeling by indole-d_5 tryptophan, and its hyperfine structure was explored by 9.5-GHz ENDOR at 10 K [34]. The obtained ^{14}N- and ^{1}H-hyperfine tensors are collected in Table 3 and the derived π-spin-densities are indicated in Fig. 3. As for the two tryptophan radicals in *E. coli* mutant Y122F, the radical in Y177W of the mouse RNR was assigned to a tryptophan neutral radical, deprotonated at the nitrogen. This was again corroborated by the detection of a small ^{1}H-hyperfine tensor assigned to a proton in a hydrogen bond to N1 (Ref. [34]; for structure see Fig. 3). Based on Eq. (3), the side chain orientation for the radical W177• in the R2 mutant Y177W of mouse RNR was determined. Based on comparison with the X-ray structure of the wild-type R2 of mouse [92], tryptophan residues in the vicinity of the diiron center were excluded, and the radical in the mutant R2-Y177W was assigned to the tryptophan residue W177• [34].

4.1.2. g-tensor from high-field EPR

EPR spectra of tyrosyl and tryptophan radicals may look very similar at conventional 9.5-GHz EPR frequency. This is demonstrated in Fig. 5, top, for the spectra from the tyrosyl radical Y177• in wild-type RNR of mouse and the tryptophan radical W177• in mouse mutant Y177W•, which both are dominated by a doublet splitting with some poorly resolved subsplitting. However, the high-field EPR spectra recorded at 94 GHz for the same radical species, shown in Fig. 5, bottom, are very different. The spectrum of the tyrosyl radical Y177• is significantly broadened and exhibits now well-resolved *g*-components (see also Fig. 4), whereas the *g*-components from the tryptophan radical W177• are still poorly resolved in the 94-GHz EPR spectra. All three *g*-tensor principal components for W177• were nevertheless determined from simulations of the 94-GHz EPR spectra (Fig. 6) using the hyperfine tensors from the previous 9.5-GHz EPR and ENDOR studies [33,34]. Simulation of the 94-GHz EPR spectrum of the tryptophan radical W111• in *E. coli* mutant Y122F, shown in Fig. 6, yielded *g*-tensor components for W111• which were within experimental error the same as obtained for W177•.

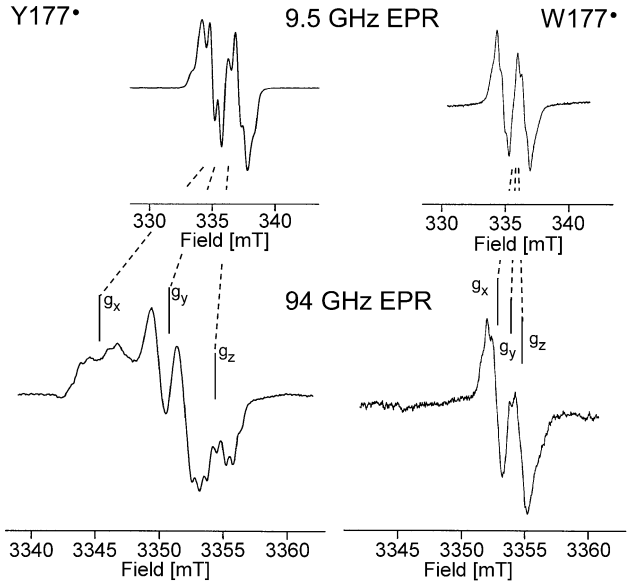

Fig. 5. Comparison of the 9.5- and 94-GHz EPR spectra of the tyrosyl radical Y177• in wild-type RNR and the tryptophan radical W177• in R2 mutant Y177W of mouse RNR [44]. The different *g*-tensor principal values ($g_{x,y,z}$, see Table 2) are fingerprints for the respective type of radical, see text. Experimental conditions: 9.5 GHz—P_{mW}, 10 μW; ma, 0.1 mT; 94 GHz—P_{mW}, 2 μW; ma, 0.4 mT; T = 20 K; see Ref. [44].

Table 2 gives a comparison of *g*-tensor values of the tyrosyl and tryptophan radicals in mutant RNR of *E. coli* and mouse. It is obvious, that the *g*-tensor of the tryptophan radicals exhibits much smaller anisotropy as that of the tyrosyl radicals. Shifts of the principal values g_x and g_y from the free electron value (g_e = 2.0023193) result from spin orbit coupling [81], which increases with increasing spin densities on heavier atoms like oxygen, due to their larger spin orbit coupling constants (see above and Ref. [54]). Therefore, radicals with large spin densities on oxygen are expected to have generally larger g_x- and g_y-components as compared with radicals exhibiting spin densities only on

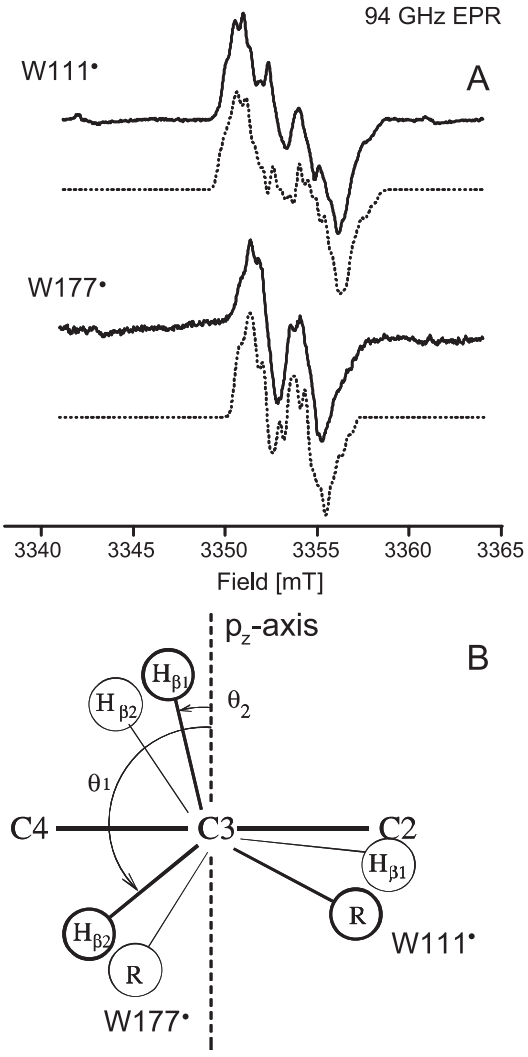

Fig. 6. (A) Comparison of the 94-GHz EPR spectra of the tryptophan radicals W111• in R2 mutant Y122F of *E. coli* RNR, and W177• in R2 mutant Y177W of mouse RNR [44]. Experimental conditions: P_{mW}, 2 μW; ma, 0.4 mT; $T = 20$ K. Dashed lines, simulated spectra, see text. (B) Edge on view of the tryptophan radical (Fig. 3) showing the side chain orientations and dihedral angles of the β-protons, deduced for both tryptophan radicals from the experimental hyperfine values of their side chain β-protons, see text. Obtained dihedral angles were $\theta_1 \approx 13°$, $\theta_2 \approx 133°$ for W111•, and $\theta_1 \approx -90°$, $\theta_2 \approx 30°$ for W177• [44].

carbon and nitrogen atoms. Furthermore, the energy gaps between the involved orbitals, e.g. non-bonding orbitals and the π-orbital carrying the unpaired electron, also determine the magnitude of spin-orbit coupling [43,82]. As a result, the observed *g*-tensor is a fingerprint for the particular type of radical and can be used for radical identification (Table 2, see below).

The situation is different for the hyperfine couplings. Fig. 6A shows a comparison of the 94-GHz EPR spectra of the tryptophan radicals W111• in *E. coli* mutant Y122F and W177• in mouse mutant Y177W. Both spectra are dominated by the large hf tensors of the β-protons from the side chain, but they look entirely different. The spectrum of W111• exhibits two large splittings, giving rise to four major lines, whereas the spectrum of W177• shows a doublet structure resulting form only one large hyperfine splitting. This demonstrates that it can be misleading to base radical identification on the hyperfine structure alone (compare Fig. 5). The *g*-tensor values, however, which were found to be identical for both radicals in Fig. 6A within experimental error (Table 2), show that both radicals are indeed the same species, which had been assigned by isotopic labeling to tryptophan radicals [33,34]. The different hyperfine couplings of the β-protons in both tryptophan radicals were a result of significantly different orientations of their side chains. These orientations were determined form the respective hf couplings according to Eq. (3) and are shown in Fig. 6B. Based on these side chain orientations, the radicals were assigned to the specific tryptophan residues, W111 in *E. coli* Y122F and W177 in mouse, by comparison with the X-ray structure of the respective wild-type enzymes [16,32–34,92].

Standard activity assays performed with the *E. coli* and mouse mutants exhibiting tryptophan radicals (Y122F, Y177W) showed no catalytic activity [33,34]. In particular for mutant Y177W of mouse RNR, where the radical W177• was assigned to the same site as the tyrosyl radical Y177• in wild type, some activity could be expected for the case that a tryptophan radical could take over the catalytic role of the tyrosyl radical. In view of the reported short lifetime (30 s) [34] and the experimental conditions for the assay (multi-turnover conditions), a possible single-turnover activity for this mutant seemed not rigorously excluded.

4.1.3. Tryptophan cation radical at W48

A tryptophan cation radical, which was assigned to residue W48, has been reported as freeze-quenched intermediate in the radical generation reaction of the diferrous iron site in wild-type R2 of *E. coli* with molecular oxygen in the absence of an exogenous source for the required extra electron [35,36]. The transient cation radical was characterized by an optical absorption band centered at 560 nm, and an EPR signal at $g \approx 2.0$ [36]. The assignment to residue W48 was based on experiments with mutant W48F [36]. No detailed hyperfine data were given for the tryptophan cation radical in [36], probably because it was generated in superposition with the EPR signal of the $Fe^{III}Fe^{IV}$ intermediate "X" [36]. While the above tryptophan neutral radicals W111• in *E. coli* and W177• in mouse were not proposed to play a catalytic role, the observation of a transient tryptophan cation radical at W48 was of particular importance, since this residue is part of the hydrogen bond pathway proposed for the catalytic radical transfer between the tyrosyl radical in R2 and C439 in R1 (see above). The radical generation reaction of the diferrous iron site with molecular oxygen requires an extra electron from an exogenous source (see above), and it was shown in Ref. [36] that the transfer of this

electron from the protein surface to the diiron site is mediated by residue W48. It has been proposed by functional models and by theoretical studies [20] that a similar cation radical W48 also emerges as intermediate during the long-range electron/proton transfer between Y122• in R2 and C439 in R1.

4.1.4. Sulfinyl radical in subunit mutant R2

In an attempt to generate a cysteine radical in protein subunit R2, the double mutant Y177F/I263C of mouse RNR has been generated. In this mutant, C263 is located at a similar distance to the diiron center as Y177 in the wild-type enzyme. The iron-oxygen reconstitution reaction was investigated by freeze-quench and subsequent EPR spectroscopy. A radical which emerged as product of this reaction was identified by 9.5-GHz EPR and by 285-GHz EPR as sulfinyl radical based on its large g-tensor components (g_x, 2.0206; g_y, 2.0093; g_z, 2.0022, see Ref. [93]). The unusual stability of the radical was explained by its hydrophobic surrounding. No catalytic activity was observed for mutant Y177F/I263C as was the case for the above described mutants with tryptophan neutral radicals. This work demonstrated, however, the ability of the enzyme to generate also cysteine-based radicals in the iron-oxygen reconstitution reaction. The observed sulfinyl radical (Cys-SO•) was considered as a stabilized form of a putative precursor thiyl (Cys-S•) radical [93].

4.2. Diiron-radical centers in mutants with hydroxylated F208 in R2 of E. coli

The iron/oxygen reconstitution and radical generation reaction in R2 (Eq. (4)) is in many aspects similar to the oxygen activation reaction in other diiron enzymes. For reviews on nonheme iron enzymes and their reactions with molecular oxygen, see Refs. [94,95]. There is a high structural similarity between the diiron centers in R2 of RNR and in the hydroxylase subunit of methane monooxygenase (MMO) [94–96] where the reaction of the diferrous iron center with molecular oxygen leads to hydroxylation of the substrate methane [94,95]. The oxygen activation reaction in MMO and its intermediates has been investigated in great detail [94,95,97].

In several mutants of *E. coli* RNR, where amino acids near the diiron site of R2 had been replaced (Y122F/E238A, F208Y, and W48F/D84E), a self-hydroxylation of an aromatic amino acid residue (F208) next to the diiron site was observed [98,99]. Apparently, small changes in the diiron ligand sphere can redirect the iron-oxygen reaction resulting in oxidation of a hydrocarbon—as in MMO—instead of radical generation, as required for RNR function. From a mechanistic point of view, these mutants are very interesting, even though they are lacking catalytic RNR active [98,99]. Double mutant W48F/D84E was engineered and its iron-oxygen reaction studied to demonstrate the change of function from RNR to MMO [99]. Based on optical absorption, and in particular on Raman spectroscopy, it was proposed that F208 was oxidized and became a phenolate, coordinated to one iron [99]. For mutants Y122F/E238A and F208Y, oxidation of F208 to a phenolate, coordinated to Fe1, was evidenced by the X-ray structure [98]. These mutants with replaced amino acids, in the iron coordination sphere, offered a unique possibility to investigate the influence of small changes in the diiron coordination on the pathway, intermediates, and products of the iron/oxygen reaction. For mutant E238A, which showed no ability to generate a radical, it was shown that proper radical generation could be restored by azide binding to the iron site. It was concluded that tyrosyl radical generation at Y122 requires a four-coordinated Fe1 and a six-coordinated Fe2 after oxygen binding to the diferrous site [100].

A new class of coupled radical-iron centers has been observed in some of these mutants. In F208Y, the iron/oxygen reconstitution reaction was reported to show a branching [101], dependent on ascorbate concentration. One branch leads to an additional oxidation of Y208 to Dopa208, which then became twofold coordinated to Fe1, as evidenced by the X-ray structure [98]. A second branch of the reaction was reported to lead to an EPR singlet signal with different saturation properties as compared with the wild-type Y122•, which was attributed to a paramagnetic center "Z". An oxo-ferryl species was proposed for "Z", possibly in equilibrium with a radical on Y208 [101].

A similar EPR signal was observed in another mutant, Y122H, originally designed to generate a histidinyl radical. Samples from the respective mutant grown on ^{57}Fe-enriched medium showed a significant isotope effect in the EPR spectra [102]. ^{1}H- and ^{57}Fe-ENDOR spectroscopy have been used to investigate the nature of this paramagnetic center "H" in mutant Y122H in more detail [102]. Fig. 7 shows pulse ENDOR spectra of this mutant in comparison with Y122• in wild-type R2 of *E. coli*. The pulse ENDOR spectrum of the tyrosyl radical Y122• in wild-type R2 (Fig. 7, trace a; data from Ref. [102]) shows lines only from ^{1}H nuclei and extends to 43 MHz. An intense and narrow feature is observed around the ^{1}H nuclear Zeeman frequency $\nu_N(^{14}N) \approx 14.5$ MHz. Several hyperfine shifted patterns according to Eq. (2) are observed. A rhombic pattern with turning points at ≈ 28 MHz (A_x) and ≈ 19 MHz (A_y) and a central peak at ≈ 24 MHz (A_z) is observed, which was assigned already in previous studies to the ring protons at positions 3 and 5 [51,52]. Another rhombic pattern is observed between ≈ 16 and ≈ 18 MHz with a low-frequency counterpart between ≈ 11 and ≈ 13 MHz. The corresponding small hf tensor was assigned already previously to the ring protons at positions 2 and 4 (Refs.[51,52]; see Fig. 3). The large hf-tensor of the β-proton of the side chain gives rise to the broad peak between ≈ 41 and ≈ 43 MHz. The obtained hf tensor values were in good agreement with those from earlier studies given in Table 1 [47,51,52].

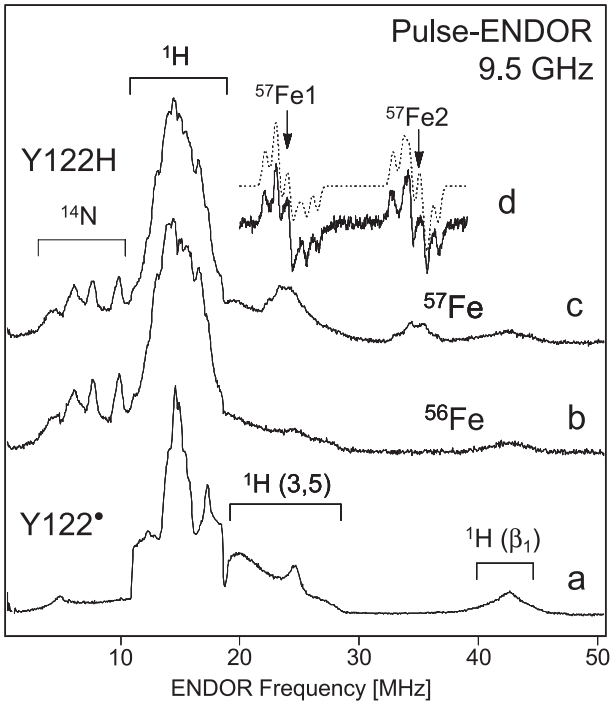

Fig. 7. 9.5-GHz Davies pulse ENDOR [58] spectra of the proposed coupled $Fe^{III}Fe^{III}$-F208-O$^{\bullet}$ (radical) center "H" in R2 mutant Y122H of *E. coli* RNR in comparison with the spectrum of the tyrosine radical Y122$^{\bullet}$ in the wild type [102], see text. Center "H" (trace b) exhibits only small ^{1}H-ENDOR splittings, but four ^{14}N-ENDOR lines. ^{57}Fe-enriched samples show two additional groups of ^{57}Fe-ENDOR lines at 24 and 34 MHz (pulse ENDOR, absorption mode, trace c; cw-ENDOR spectrum in first derivative mode for better resolution, trace d). Traces a–c: microwave ESR pulses, 192, 96, 192 ns; radio frequency (rf) NMR pulse, 8 μs; T = 10 K. Trace d: cw-ENDOR, P_{mW}, 8 mW; P_{rf}, 150 W; ma, 150 kHz; T = 8 K. Dotted trace, simulation [102]. ^{57}Fe hf-tensor values, see Table 4.

In contrast to the tyrosyl radical Y122$^{\bullet}$, the ENDOR spectrum of the paramagnetic center "H" in mutant Y122H (Fig. 7, trace b) shows only small ^{1}H hyperfine splittings, giving rise to the broad poorly resolved intense structure restricted to the spectral region between 11 and 18 MHz. The corresponding hyperfine couplings were all ≤7 MHz. However, there were four additional lines in the spectrum of "H", between 5 and 10 MHz, which were absent in Y122$^{\bullet}$. They were assigned to the two ^{14}N nuclei, from histidines H118 and H241 [102] which coordinate to the two irons; see Fig. 2. Similar ENDOR lines have been observed for the diiron site of the structural similar enzyme MMO, which is also coordinated by two histidines [94,103]. In ^{57}Fe-enriched samples, two additional strong groups of ^{57}Fe ENDOR lines were observed centered about ≈24 and ≈36 MHz (Fig. 7, trace c). According to Eq. (2), each of the two groups of lines is made up of three pairs of lines, centered around the respective ^{57}Fe hf-tensor principal components A_j ($j = x, y, z$), and separated by $2\nu_N(^{57}Fe) \approx 1.8$ MHz. Simulation of the ^{57}Fe-ENDOR spectra recorded in the continuous wave (cw) first derivative mode (dotted line, trace d) yielded all three principal components of two ^{57}Fe hyperfine tensors, which are collected in Table 4 [102]. The two large ^{57}Fe hf tensors clearly show the involvement of the two irons in center "H".

The cw-ENDOR spectra for "H" in Y122H and intermediate "X" in wild-type R2 are compared in Fig. 8 (Ref. [104], M. Kolberg, D.T. Logan, G. Bleifuss, S. Pötsch, A. Gräslund, W. Lubitz, G. Lassmann, and F. Lendzian, (2004), submitted to J. Biol. Chem.). Intermediate "X" has been investigated extensively earlier by 35-GHz ENDOR [27,28] and was identified as an antiferromagnetically coupled $Fe^{III}Fe^{IV}$ center with a total electron spin $S = 1/2$. A structural model for the intermediate "X" based on the X-ray structure of an azide complex of R2 was given in Ref. [105]. The groups of ^{57}Fe ENDOR lines at ≈36 MHz are very similar in the spectra of "X" and "H" in Y122H (Fig. 8c and d), both with respect to their frequencies and the observed subsplitting. The obtained ^{57}Fe hf tensor values, assigned to Fe2, are given in (Table 4). The low hyperfine anisotropy was consistent with a high spin ($S = 5/2$) Fe^{III} state [27,28,106]. However, there is a significant difference between the two smaller ^{57}Fe hf-tensors of "X" and "H" in Y122H, with corresponding groups of lines at lower frequencies of ≲25 MHz (see Fig. 8, traces c, and d). This smaller ^{57}Fe hf tensor was assigned in "X" to the Fe^{IV} ion [28] and has for "X" much smaller but more anisotropic components than observed for "H" in Y122H (compare Table 4). Generally, for high spin $^{57}Fe^{III}$, only small hyper-

Table 4
g-tensor and ^{57}Fe-hf tensor principal values [mT] of the diiron radical center "H" ($Fe^{III}Fe^{III}$-F208$^{\bullet}$) in mutant Y122H RNR and of the $Fe^{III}Fe^{IV}$ intermediate "X" of *E. coli*

Paramagnetic center[a]	Tensor element	*g*-tensor	^{57}Fe-hf tensor Fe2		^{57}Fe-hf tensor Fe1[b]	
"H"	*x*	2.0088(1)	Fe^{III}	2.59(1)[b]	Fe^{III}	1.86(1)[b]
($Fe^{III}Fe^{III}$)	*y*	2.0040(1)		2.49(1)		1.70(1)
-F208-O$^{\bullet}$	*z*	1.9960(2)		2.38(1)		1.61(1)
in *E. coli* Y122H [102]						
"X"	*x*	2.007	Fe^{III}	2.65[c]	Fe^{IV}	0.98[c]
($Fe^{III}Fe^{IV}$)	*y*	1.999		2.58		1.31
in *E. coli* Y122F [28]	*z*	1.994		2.61		1.31

[a] "H" is proposed to be a three-spin ($S_1 = 5/2$, $S_2 = 5/2$, $S_3 = 1/2$) system [102], "X" is a two-spin (S1 = 5/2, S2 = 2) system [28]. Both centers show antiferromagnetic coupling and have an $S = 1/2$ ground state, see text.

[b] Absolute values sorted by magnitude, 1 mT = 28.0 MHz. Assignment to Fe1 or Fe2 (Fig. 2) could be exchanged [102]. A three-spin coupling model predicts spin projection factors, to which the isotropic ^{57}Fe hyperfine values are proportional, of 7/3 ($^{57}Fe2^{III}$), −14/9 ($^{57}Fe1^{III}$), and 2/9 (radical$^{\bullet}$) for the antiferromagnetically coupled ($Fe^{III}Fe^{III}$)-radical$^{\bullet}$ system "H" [102,106], in good agreement with the experimental ^{57}Fe-hf tensor values; see text.

[c] Spin projection factors, 7/3 ($^{57}Fe2^{III}$) and −4/3 ($^{57}Fe2^{IV}$), in agreement with the experimental ^{57}Fe-hf tensor values [28].

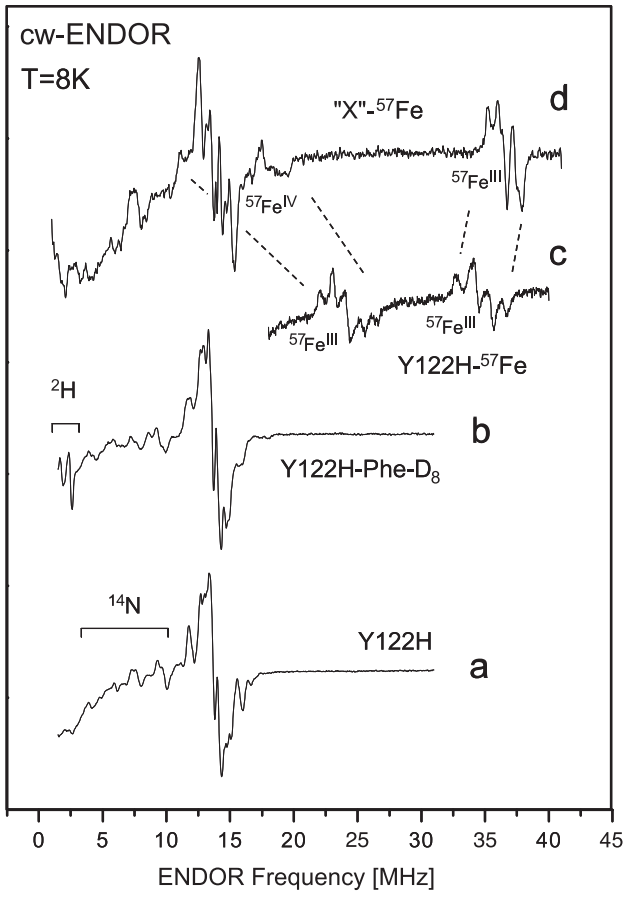

Fig. 8. cw-ENDOR spectra (first derivative mode) of the proposed diiron radical center $Fe^{III}Fe^{III}$-F208-O$^{\bullet}$ in R2 mutant Y122H (traces a–c) and of the intermediate $Fe^{III}Fe^{IV}$ center "X" in Y122F (trace d). P_{mW}, 8 mW; P_{rf}, 150 W; ma, 150 kHz; T=8 K. Spectra from samples with selectively labelled phenylalanine (Phe-D_8) show changes in the ^{1}H-ENDOR range and additional ^{2}H-ENDOR lines (trace b). An oxidized phenoxyl radical at F208 was proposed for the radical site in Y122H (Refs. [104,107], M. Kolberg, D.T. Logan, G. Bleifuss, S. Pötsch, B.M. Sjöberg, A. Gräslund, W. Lubitz, G. Lassmann, and F. Lendzian, (2004), submitted to J. Biol. Chem.), see text. The groups of ^{57}Fe-ENDOR lines of "H" in Y122H (trace c) and "X" (trace d) at ≈ 34 MHz with corresponding ^{57}Fe-hf tensor values of ≈ 2.5 mT (Table 4, 1 mT = 28.0 MHz) are assigned in both systems to high spin Fe^{III}. The second group of ^{57}Fe ENDOR lines (≈ 24 MHz in Y122H (trace c) and 11–18 MHz in "X" (trace d), with corresponding different ^{57}Fe-hf tensor values (Table 4) were assigned to high spin Fe^{III} for "H" in Y122H, and to high spin FeIV for "X" [28,102], see text.

fine anisotropy is expected, since each d-orbital is occupied by one single electron, resulting in an almost spherical spin distribution [28,106]. Therefore, both ^{57}Fe hf tensors of "H" in Y122H were assigned to $^{57}Fe^{III}$. In order to explain the observed overall S=1/2 spin state, a coupled $Fe^{III}Fe^{III}$-radical center was proposed for "H" in Ref. [102].

Recently, it was shown by ^{1}H and ^{2}H ENDOR experiments on Y122H with selectively ^{2}H-labeled phenylalanines (Phe-D_8) that the radical in center "H" resides on a phenylalanine (Refs. [104,107], M. Kolberg, D.T. Logan, G. Bleifuss, S. Pötsch, B.M. Sjöberg, A. Gräslund, W. Lubitz, G. Lassmann, and F. Lendzian, (2004), submitted to J. Biol. Chem.). Fig. 8, trace b, shows a cw-ENDOR spectrum of a labelled Phe-D_8 sample of Y122H with an additional pair of ^{2}H ENDOR lines centered around 2.2 MHz, which result from ^{2}H-phenylalanine. Since the formation of a phenyl radical seemed unlikely, it was proposed that F208, which is the phenylalanine closest to the irons, becomes in Y122H hydroxylated, like it was observed for mutant Y122F/E238A [98], and further oxidized to a phenoxyl radical, which is then probably coordinated to one of the irons [102,104,107]. The observed magnitudes of both ^{57}Fe hf tensors in "H" of Y122H (see Table 4) as well as the small magnitude of the hyperfine values from the phenoxyl radical on F208 were in good agreement with a three-spin coupling model for such a spin system (S=5/2 for each of the high spin Fe^{III} and S=1/2 for the radical) [106], which predicts large spin projection factors (7/3 and −14/9) for the two Fe^{III} and only a small spin projection factor (2/9) for the radical [102,106]. The proposed Fe^{III}-Fe^{III}-F208 phenoxyl radical center for Y122H is further supported by the strong similarity of its ENDOR spectrum with that recorded in our laboratory from center "Z" in mutant F208Y (data not shown), where the phenylalanine is replaced by a tyrosine. Studies on mononuclear iron model complexes have shown that a Fe^{III} complex with phenoxyl radical ligands can indeed be rather stable [108].

Comparison of Figs. 7 and 8 shows that an antiferromagnetically coupled $Fe^{III}Fe^{III}$-tyrosyl radical (S=1/2) spin system exhibits an ENDOR spectrum more similar to that of a $Fe^{III}Fe^{IV}$ (S=1/2) system but very different from that of a free tyrosyl radical. Mutants with such diiron-radical centers do not show catalytic activity. However, they indicate how small changes in the iron coordination sphere can change significantly the reaction of the diiron center with molecular oxygen. They may also serve as models for coordinated radical-metal centers e.g. in galactose oxidase [109,110], or in other metal enzymes, where such centers were proposed as functional intermediates.

5. High-field EPR on Y122$^{\bullet}$ in R2 single crystals from wild-type *E. coli*

5.1. Structural changes induced by tyrosyl radical formation

Crystal structures of *E. coli* R2 are available for both the reduced diferrous ($Fe^{II}Fe^{II}$-Y122-OH) form [111] and the diferric, met form lacking the radical ($Fe^{III}Fe^{III}$-Y122-OH) [16]. The structural data has together with kinetic data, and theoretical calculations, served as the basis for the formulation of mechanistic proposals for the radical generation in R2 as well as for the radical migration from Y122$^{\bullet}$ in R2 to C439 in R1 in the catalytic reaction [1–5,8,18–23]. The radical migrations involve coupled electron/proton transfer reactions, which are expected to be very sensitive to the structure and distances of the reaction partners. However, no

structure has been available for the radical containing form of R2, because the tyrosyl radical Y122• is too short-lived to survive crystallization of the protein.

The problem of the amount of displacement of the tyrosine Y122 upon radical formation has been investigated recently in a combined high-field EPR and high-resolution (1.4 Å) X-ray single crystal study by Högbom et al. [49]. In that work, the orientation of the *g*-tensor of the radical Y122• in the crystal was determined with high precision by single crystal high-field EPR. The *g*-tensor axes of the tyrosyl radical are collinear with its molecular axes (Fig. 3) as shown in a previous study on irradiated tyrosine crystals [53]. The radical Y122• was generated in single crystals of R2 both by the shunt reaction of met-R2 ($Fe^{III}Fe^{III}$-Y122-OH) with H_2O_2 [112] and by the iron/oxygen reconstitution reaction [24] with crystals of the apoprotein as described in [49]. Both methods have been used previously for R2 protein solutions to generate the tyrosyl radical and restore catalytic activity [24,112]. The estimated radical yields in the crystals, ≳10%, were too low for determining the X-ray structure for the radical state, but sufficient to obtain well-resolved single crystal EPR spectra with good signal to noise ratio. Large crystals ($\approx 0.7 \times 0.3 \times 0.2$ mm^3) suitable for single crystal EPR were grown from met-R2. They were mounted to a high precision EPR quartz capillary and then soaked with H_2O_2 and shockfrozen in liquid nitrogen.

94-GHz high-field EPR spectra were recorded for these R2 single crystals and a full 180° rotation pattern of the spectra in 7.5° steps is shown in Fig. 9 (black traces). The spectra were analyzed with a program, which enabled simultaneous simulation of the spectra for all eight sites in the crystal and for all orientations [49]. This was achieved using a spin Hamilton operator, which was based on the same electron Zeeman, nuclear Zeeman, and hyperfine terms, as in Eq. (1), but extended by the crystal symmetry operations known from the X-ray structure analysis. In this way, spectra for all four magnetically inequivalent sites of the crystal (orthorhombic space group $P2_12_12_1$) for both chains A and B of the protein homodimer were simultaneously generated. In addition, a simulated annealing and fit routine was included in order to find the global minimum for the fitting process [49]. The analysis yielded the orientation of the *g*-tensor axes in the crystal axis system and the orientation of the crystal axes in the laboratory frame. The latter was additionally verified by X-ray diffraction of the same crystal mounted to the EPR capillary [49]. The finally obtained best simultaneous fit for all spectra and all orientations of Y122• in the R2 single crystal is shown in Fig. 9 (light blue-grey traces). Effective *g*-values for each site in the protein chain A and B are also indicated (cosine patterns in different colors).

Analysis of these data revealed several interesting results: The obtained principle values of *g*- and hyperfine tensors were the same as in frozen protein solution (see Tables 1 and 2, and Fig. 9, caption), indicating that the tyrosyl radical generated with H_2O_2 in the crystal had the same structure

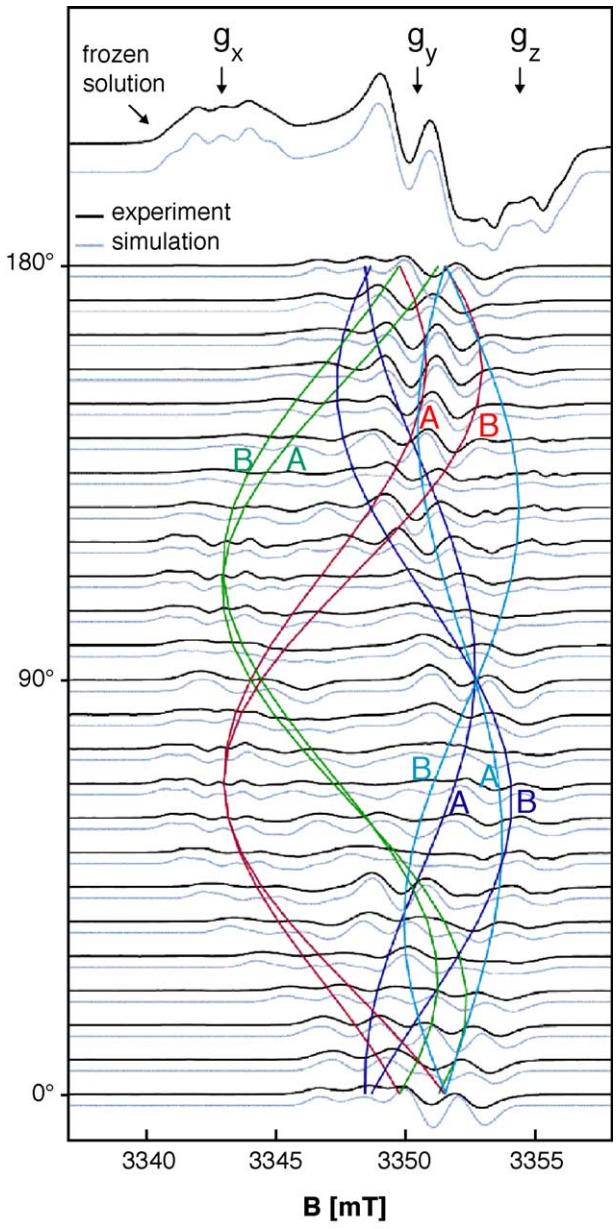

Fig. 9. 94-GHz EPR spectra (black experiment, grey simulation) of Y122• in R2 frozen solution (top trace) and of Y122• generated with H_2O_2 in a R2 single crystal from RNR of *E. coli* [49]. Full 180° rotation pattern recorded in 7.5° steps (see text). Colored cosine patterns indicate the angular dependence of the effective *g*-values for all four sites in the unit cell (space group $P2_12_12_1$) for both protein chains A and B (see text, data adopted from Ref. [49]). The same *g*-tensor parameters were obtained from simulations of protein frozen solution and single crystal spectra (top two traces, for *g*-values see Table 2). The hf-tensor values obtained from simulations were: −0.97(6), −0.28(6), and −0.74(6) mT for $A_{x,y,z}$, respectively, of positions 3 and 5, see Fig. 3; numbers in brackets are errors in the last digit; *x*- and *y*-axes were rotated by +24° (position 3) and −24° (position 5) with respect to the *g*-axes; and 2.10(6), 1.85(6), and 1.96(6) mT for $A_{x,y,z}(H_{\beta 1})$, in good agreement with Refs. [44,47,51]. Experimental conditions: P_{mW}=2 μW; ma, 0.2 mT; T=80 K.

and the same hydrophobic environment (no hydrogen bond, see above) as in active enzyme solutions. The simulations showed that 60–70% of the relative radical yield was

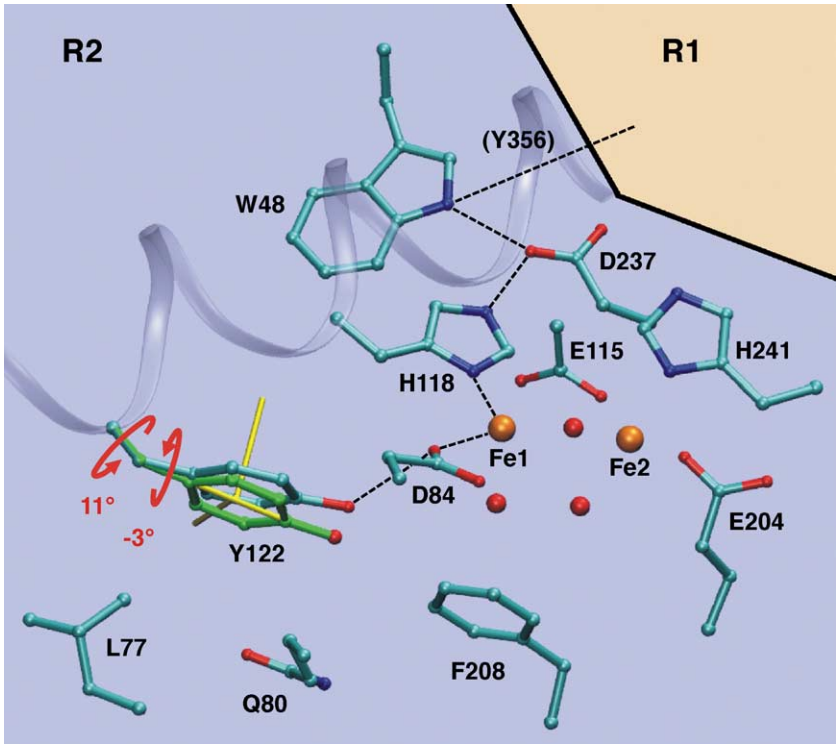

Fig. 10. X-ray structure [16,49] of met-R2 ($Fe^{III}Fe^{III}$-Y122-OH) showing the diiron site and its amino acid environment together with the hydrogen-bonded conserved amino acid residues making up the proposed electron/proton transfer pathway [1–5,8] between the diiron site in R2 and the substrate binding site in R1. Green: orientation of the radical $Y122^{\bullet}$ and its *g*-tensor axes (yellow) as obtained from the single crystal EPR analysis (Fig. 9). The radical orientation deviates from that of the reduced tyrosine (X-ray structure), and can be obtained by 11° and −3° free bond rotations (red) around $C_\alpha-C_\beta$ and $C_\beta-C_1$, [49]. This conformational change disconnects the tyrosyl radical oxygen from the hydrogen bond pathway, see text.

observed in protein chain A and only 30–40% in chain B. Interestingly, the maximum radical yield determined from reconstituted frozen solutions of R2 was also reported to have a nonstoichiometric value of ≈ 1.2 per protein dimer [113].

The key result of that single crystal EPR study was, however, the orientation of the *g*-tensor axes and hence those of the radical $Y122^{\bullet}$ with respect to the X-ray structure of Y122-OH in met R2. The radical $Y122^{\bullet}$ was found to be rotated with respect to the reduced tyrosine, Y122-OH), leading to angles of 10°, 8°, and 5° (errors ± 1°)[1] between their respective molecular *x*, *y*, and *z* axes (see Fig. 3 for axes). For an estimation of the location of the radical, it was assumed that the origin of the measured rotation was in the flexible tyrosine side chain and that no energy costly translational motion of the helix backbone should occur. The energetically most favorable way to obtain the observed radical orientation within less than 2° was by rotations of 11° about the $C_\alpha-C_\beta$ and −3° about the $C_\beta-C_1$ bonds. Fig. 10 shows the obtained location of the radical $Y122^{\bullet}$ for these rotations. It is noteworthy that the larger rotation of 11° about $C_\alpha-C_\beta$ does not affect the dihedral angles for the β-protons; see above. The rotation about $C_\beta-C_1$ (Fig. 3), which changes these dihedral angles, was only −3°, and too small for a significant change of the isotropic hyperfine coupling $A_{iso}(H_{\beta 1})$ of the β-protons; compare Eq. (3). This finding was in line with the earlier conclusion that the hyperfine coupling of the β-proton agrees with the X-ray structure of the reduced tyrosine Y122-OH [51,52].

In this model, the radical was found to be rotated away from the diiron center, as compared with the reduced tyrosine; see Fig. 10. The largest displacement was found for the tyrosine oxygen. In the met form of R2 ($Fe^{III}Fe^{III}$-Y122-OH, X-ray structure), the oxygen of the reduced tyrosine has a distance of about 3.2 Å from one of the oxygens of Asp84, probably forming a weak H-bond [16,49]. The rotation of the radical increased this distance to over 4 Å, which is too far for hydrogen bonding to Asp84. This finding was consistent with the large g_x-component ($g_x = 2.00912$) observed for $Y122^{\bullet}$ both in frozen solution and in the crystal, and which is indicative

[1] The small error is due to the fact that the information on the relative orientations of *g*-tensor and crystal axes systems is contained in the spectra and does not require similar high precision for crystal mounting [49]. The error was estimated from several fit and annealing procedures and from simulations using deviating angles. In theoretical studies, the g_x axis is reported to be collinear with the tyrosine C=O bond orientation [84]. EPR studies on irradiated tyrosine crystals indicate only small deviation of the g_x axis from the C=O axis (≲2° as estimated from Fig. 5 in Ref. [53]).

of a nonpolar and not hydrogen bonding environment [42–44,47,49,65].

The observed displacement of the tyrosine oxygen has probably functional implications. The radical transfer path between Y122• in R2 and C439 at the active site in R1 has been suggested to involve in R2 the conserved residues D84, H118, D237, and W48, depicted in Fig. 10, and Y730 and Y731 close to the active site C439 in R1 [1–5,16,17], see Fig. 2. Most of these residues form conserved hydrogen bonds, which served as a basis for detailed proposals for a coupled proton/electron transfer mechanism along this chain [1–5,8,18–21,21–23]. It has been proposed in a theoretical study that the first step of the long-range radical transfer reaction is a transient hydrogen atom abstraction from the water coordinated to Fe1 (Fig. 10) by the radical Y122•, and subsequent formation of a radical character on W48 within one step [20]. The location of the reduced tyrosine, Y122-OH, shown in the X-ray structure of met-R2, Fig. 10, cyan, may be similar to that of the transient state of this proposed hydrogen abstraction reaction, where Y122• becomes transiently reduced to Y122-OH. The observed conformational change, coupling or uncoupling Y122 from the metal site and from the hydrogen bond network, may assist in controlling this reversible protonation/deprotonation reaction.

Similar small conformational changes, which are sufficient to form or to break hydrogen bonds, may occur during the long-range electron/proton transfer also for other amino acids along the hydrogen bond pathway, a process which may be supported by protein structural fluctuations proposed in mechanistic models for this reversible radical transfer reaction [22,23], which performs over a remarkable distance of 35 Å and bridges two protein subunits [1–5,8]. The combined high-field EPR and X-ray single crystal study [49] demonstrated that small conformational changes upon radical formation (10° rotations) can be resolved by this approach.

6. Radicals in subunit R1 of RNR of *E. coli*

6.1. Inhibitor radicals in R1

Mechanism-based inhibitors were designed, which bound like the substrate, but performed only part of the substrate turnover reaction leading to rather stable inhibitor radicals fixed in the substrate binding pocket, which blocked further RNR activity [1,5,8,114–120]. The substrate analogues acting as inhibitors had antiviral and antitumor activity and were found to be important for the design of mechanism based new inhibitors of RNR [8]. The study of various substrate-analogue inhibitors was a powerful tool for investigating the substrate turnover cycle in subunit R1 [1,5,8,114–120]. In these studies, besides the inhibitor radicals, also protein-based radicals in R1, e.g. dithiyl radicals (R-SS•), were observed [120]. Kinetic studies showed that the inhibitor radical intensities build up in subunit R1 on the expense of the tyrosyl radical signal from subunit R2, which was strong evidence for the proposed radical transfer mechanism involving both, R2 and R1 [1,5,8,114–120]. The studies of such inhibitor radicals constitute its own field and are beyond the scope of this report on amino acid radicals in class I RNR. For reviews and recent high-field EPR studies, the reader is referred to Refs. [1,5,8,40,47,114–120].

6.2. Thiyl radicals from cysteines in proteins

The widely accepted mechanistic model for RNR function involves a long-range electron/proton (radical) transfer from the tyrosyl radical Y122• in R2 to C439 at the substrate binding site in R1 [1–5,8]. The putative thiyl radical C439 is then believed to attack the substrate and start the turnover reaction by abstracting the 3′H-atom [1,8]; see Fig. 1. There is strong indirect evidence for the involvement of the thiyl radical at C439 from studies on mechanism-based inhibitors (see above) and from the observation of a thiyl radical, coupled to cobalamin in class II RNR [12–14]. So far, the putative thiyl radical at C439 in R1 has, however, not been observed. For its detection and identification, it was important to characterize spectral properties of thiyl radicals by EPR. Thiyl radicals, generated in cysteine and other thiols by irradiation with UV at low temperatures, had been investigated by 9.5-GHz EPR [121]. They exhibited EPR properties quite unusual and differing from those of aromatic amino acid radicals. Their g-tensor is very anisotropic with a $g_{\perp}$-value of ≈ 2.00 and a $g_{\parallel}$-value as large as ≈ 2.3 [121]. This was attributed to the larger spin orbit coupling constant of sulfur (383 cm^{-1}) [54] as compared with carbon, nitrogen or oxygen (see above) and to the near degeneracy of the sulfur orbitals [121,122].

Protein-based thiyl radicals have been artificially generated by low temperature ($T = 77$ K) UV irradiation and investigated by 9.5-GHz EPR [123]. Fig. 11 shows EPR spectra obtained from UV irradiated bovine serum albumin (BSA, trace b) as model protein, and R1 (trace c) in comparison with polycrystalline cysteine (trace a). The obtained $g_{\parallel}$-values were ≈ 2.3 for the thiyl radicals in polycrystalline cysteine and 2.18 for the thiyl radicals in BSA. The difference of the $g_{\parallel}$-values for polycrystalline cysteine and for BSA was attributed to the presence of hydrogen bonding for the thiyl radicals in BSA. This was expected to lower the energy of orbitals involved in hydrogen bonding, thereby lifting degeneracy of sulfur non-bonding orbitals and reducing the g-anisotropy, similar to what was observed for tyrosyl radicals (see above), but much more pronounced [123]. Recent theoretical g-tensor calculations for thiyl radicals are in good agreement with the experimental values [124]. A broad $g_{\parallel}$-feature, extending from ≈ 2.3 to ≈ 2.15, was found for the thiyl radicals in R1, which is barely seen in trace c, but became more evident in integrated spectra [123]. This broadening

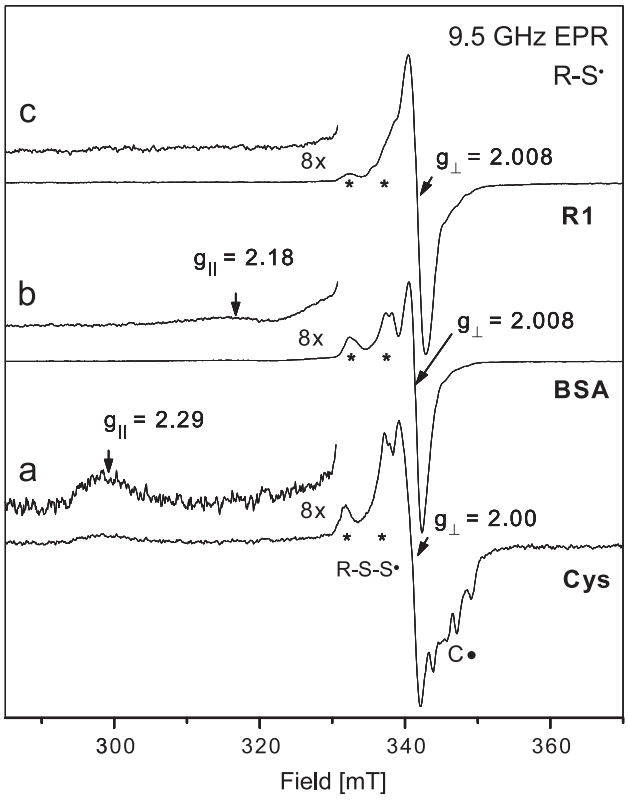

Fig. 11. 9.5-GHz EPR spectra of thiyl radicals in UV-irradiated frozen aqueous solutions of R1 protein of *E. coli* RNR (0.5 mM, trace c), bovine serum albumin (BSA, 4 mM, trace b) and cysteine (300 mM, trace a). All samples anaerobic, UV irradiated at $T = 77$ K. Trace a: P_{mW}, 0.1 mW; $T = 10$ K. Traces b and a: P_{mW}, 200 mW; $T = 80$ K. (Adopted from Ref. [123].) Cysteine: non-H-bonded, $g_{\|} = 2.29$; BSA: H-bonded, $g_{\|} = 2.18$; R1: 11 cysteines per R1 monomer, heterogeneous H-bonds, see text. Dithiyl radicals indicated by asterisks.

was attributed to heterogeneous hydrogen bonding for thiyl radicals from the 11 cysteines [17] found in each monomer of the R1 protein. The protein-based thiyl radicals were found to exhibit anisotropic EPR relaxation with half saturation powers much larger than those for aromatic amino acids [123,124]. Consequently, they were detectable by EPR only at low temperatures < 150 K. The radicals were found to be stable only at low temperatures up to 170 K [123].

Low-temperature UV-irradiation was a nonspecific method, which generated also traces of carbon centered radicals; see Fig. 11, trace a. Furthermore, thiyl radicals could be also expected from methionines [123]. Two specific methods for generation of thiyl radicals only from cysteines in protein liquid solutions have been used: (i) chemical oxidation of cysteines with Ce^{IV}/nitrilotriacetate (NTA) and (ii) laser flash photolysis of R1 and BSA, where the cysteines had been previously nitrosylated with *S*-nitrosopenicillamine (SNAP), thereby generating RSNO groups, from which the NO was then flashed off [125]. Both methods have been applied for BSA and R1 and transient thiyl radicals were indirectly evidenced by EPR using the spin trap technique, where the intermediate thiyl radical was transformed in a chemical reaction with a spin trap to a stable spin adduct radical [125]. These adduct radicals, however, gave no information on the yield and lifetime of the thiyl radical precursor. Recently in our laboratory, chemical oxidation with Ce^{IV}/NTA was used in combination with rapid freeze quench techniques and subsequent low temperature EPR. These experiments (data not shown) indicate a room temperature lifetime of 1–2 s for the protein-based thiyl radicals in the model protein BSA.

These studies on artificial thiyl radicals in proteins characterized their EPR spectra and lifetimes. However, they were generated randomly from all cysteines. For proving the functional model for RNR, the future challenge will be to artificially generate a thiyl radical specifically at C439 and then prove its functional capability for substrate turnover.

6.3. Cysteine-based radicals during substrate turnover in mutants of R1

Site-directed mutagenesis has been applied as a second approach besides the use of mechanism-based substrate analogue inhibitors (see above) to investigate the turnover reaction in R1 in solutions of the holoenzyme. A detailed model for the substrate turnover cycle was proposed based on the experiments with mechanism-based inhibitors [8], where amino acid residues, in particular cysteines C225, C462, and E441, were involved in deprotonation/protonation reactions with the substrate [1,8,126]. Recently, R1 mutant E441Q, which is in close proximity to the substrate (see Fig. 2), was prepared and investigated by two groups in order to explore the role of this amino acid in more detail [39,40,126]. Two subsequent radicals were detected by 9.5-GHz EPR in holoenzyme samples, which had reacted with substrate (cytosine diphosphate, CDP) and were subsequently frozen after different incubation times. The first radical detected on a time scale of seconds was assigned in Ref. [39] to a cysteinyl radical based on isotopic labeling; the second radical observed on a minute time scale was assigned to a substrate derived radical [39,126].

A high-field 140-GHz pulse EPR study has been performed on R1 mutant E441Q, by which the proposed transient cysteinyl radical [39] was characterized in more detail [40]. 140-GHz pulse EPR spectra obtained from E 441Q R1–R2 holoenzyme samples freeze-quenched after 10 s are shown in Fig. 12. Three different radicals contributed to these spectra. Their individual contributions could be separated using high-field pulse EPR techniques taking advantage of the different spin relaxation times of the radicals (Ref. [40], see above). For reviews on pulse EPR and ENDOR methods, the reader is referred to Ref. [58–61].

The spectra shown in Fig. 12 were obtained by recording the intensity of the EPR spin echo [58,61] signal as function of the magnetic field [40]. The echo signal occurs with a delay time τ_1 (230 ns) after the third microwave pulse (see

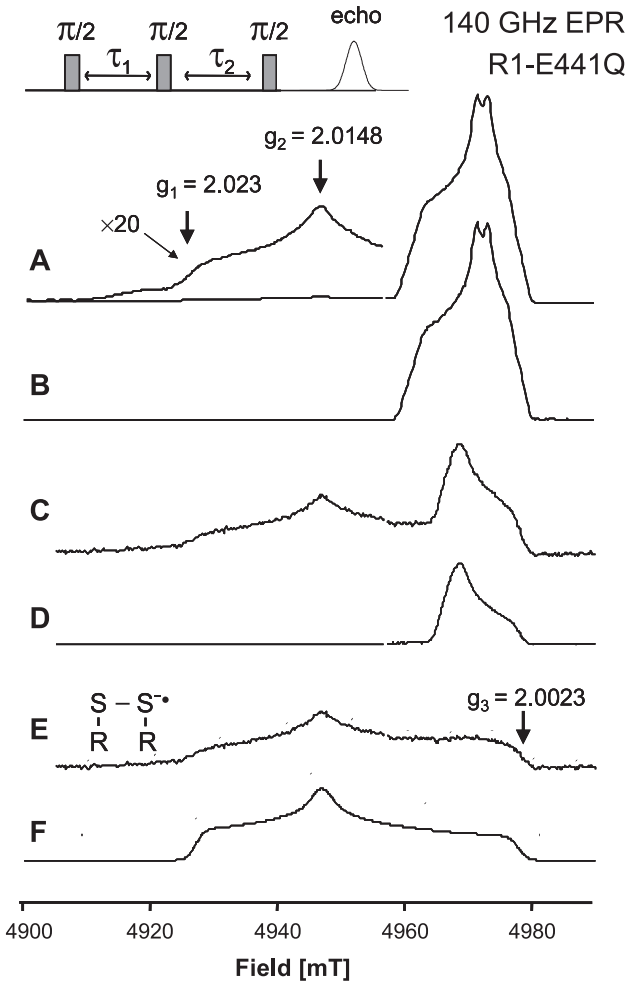

Fig. 12. 140-GHz pulse EPR spectra of RNR R1 mutant E441Q of *E. coli*. Data from M. Bennati, private communication [40]. Reaction of R2 and R1 with substrate freeze-quenched after 10 s (A–C). Insert: microwave pulses, $\tau_1=\tau_2=230$ ns. (A) $T=20$ K, showing Y122$^\bullet$ in R2 and RSS$^-$ $^\bullet$R in R1. (B) Y122$^\bullet$ in R2 alone. (C) $T=60$ K, showing RSS$^-$ $^\bullet$R and a substrate derived radical. (D) Reaction freeze-quenched after 5 min, only the substrate-derived radical is observed [40]. (E) Traces C–D.

insert, top), and the contributions of the different radical species to this echo signal decay during the time interval τ_2 by their individual spin relaxation times T_2 (Refs. [58–61], see above). At $T=20$ K (trace A), the spectrum is dominated by the strong signal of the tyrosyl radical Y122$^\bullet$ in subunit R2. The pure spectrum of Y122$^\bullet$ from a frozen R2 solution is shown in trace B for comparison. The weak EPR spectrum of a second radical species is seen on the low-field side of trace A, insert, with higher amplification. It is known that the spin relaxation time of the tyrosyl radical Y122$^\bullet$ becomes very short at increased temperatures, due to the magnetic coupling to the diferric iron center, which is at low temperature in the $S=0$ ground state, but acquires increasing paramagnetic character at higher temperature due to population of higher spin states [30]. Trace C shows the pulse EPR spectrum obtained at $T=60$ K. No signal from the tyrosyl radical was observed in this spectrum, since its spin relaxation time T_2 was now short as compared with the echo delay time τ_2 (insert, top), which prevented formation of a spin echo. The spectrum of the second radical, which exhibited long relaxation times also at $T=60$ K, is still present on the low-field side. On the high-field side, now a third spectrum is seen, which was attributed to a not fully identified substrate-derived radical [40]. This substrate-derived radical was the only remaining species observable at $T=60$ K after 3-min incubation at room temperature, trace D. Trace E shows the pure spectrum of the first intermediate radical species obtained by subtraction of traces C and D. The obtained *g*-values for the first radical intermediate (after 10-s incubation, trace E) were: $g_1=2.023$, $g_2=2.0148$, and $g_3=2.0023$ [40].

There are several structurally different radicals that may be derived from cysteines, which all have different *g*-values by which they can be identified. Besides the thiyl radical R-S$^\bullet$ with $g_1=2.18-2.3$, $g_2=g_3\approx 2.00$, see above [121–123], these are the dithiyl radical, R-S-S$^\bullet$, with $g_1=2.052-2.062$, $g_2=2.023-2.027$, $g_3\approx 2.00$ [121,123,127], the sulfinyl radical, R-SO$^\bullet$, which may emerge in case of aerobic conditions, with $g_1=2.0206$, $g_2=2.0093$, $g_3=2.0022$ [93,125,127], and the charged disulfide anion radical, R-S-S$^-$ $^\bullet$-R, with $g_1=2.0017-2.0024$, $g_2=2.0014-2.0020$, and $g_3=2.002$ [127,128]. By comparison with the *g*-values of these species, the first intermediate (10-s incubation) radical species in E411Q was identified as a disulfide anion radical [40] which was assigned to the adjacent cysteines C225 and C462 next to the substrate (see Fig. 2). Both cysteines were long known to be involved in the substrate turnover reactions, since they form a disulfide bond in the course of the reaction and have to be reduced with the help of thioredoxins before a new substrate molecule can bind [1,8]. The observed disulfide radical has been proposed as an intermediate during the substrate reaction in a detailed model for the substrate turnover cycle [8,126] and more recently also from theoretical DFT studies [19,129].

The high-field EPR study on E441Q [40] represents a beautiful example how different radical species can be separated by combining high spectral resolution and time resolution in pulse high-field EPR. They enabled the clear identification of the disulfide anion radical (C225 and C462) as an important intermediate of the substrate reaction cycle.

7. Outlook

Redox active amino acid radicals occur as intermediates in different reactions of class I RNR: in the radical generating iron/oxygen reconstitution reaction in subunit R2 (Eq. (4)), in the electron/proton (radical) transfer reaction between Y122$^\bullet$ in R2 and C439 in R1 (Fig. 2), and during the substrate turnover reaction in subunit R1. This short review intended to show that high-field EPR and ENDOR spectroscopies are important tools for the investigation of radical intermediates in all these reactions. The presented examples

demonstrated how different amino acid radicals could be identified based on their *g*-values [40–44]. Assignments to specific residues could be achieved using the information of the side chain orientation, which was obtained from the hyperfine splittings of hydrogen atoms of the side chain [32–34]. Furthermore, interactions with the environment could be sensed by changes in the *g*-tensor values [43,44,47,48,65,82], in particular hydrogen bondings, which are important for the proposed electron/proton transfer mechanism, and may be expected to also influence redox potentials and reactivity. Coupled diiron radical centers, which were observed in R2 mutants showing hydroxylation of F208, were identified and characterized by ^{57}Fe-ENDOR [102]. Overlapping spectra from tyrosine, disulfide and substrate-derived radicals in samples of the R1–R2 complex were separated by combining the enhanced spectral resolution and time resolution using pulse high-field EPR techniques at 140 GHz [40]. High-field EPR experiments on the tyrosyl radical generated in R2 single crystals yielded for the first time information on the amount of conformational change of the tyrosine upon radical formation [49]. Such conformational changes may also occur during the coupled electron/proton (radical) transfer from Y122$^{\bullet}$ in R2 to C439 in R1.

Future studies will certainly extend the structural information on the amino acid radicals by increasing applications of advanced EPR techniques. Further high-field EPR studies on trapped short-lived intermediates in RNR single crystals, which might be generated only with low yield, will deliver important structural information, which will supplement the information from X-ray crystallography on the more stable states. Advanced pulse EPR methods will extend the obtained information towards dynamics. Pulse EPR was shown to yield information on the time scale and amplitudes of libration motion of radicals [59]. Furthermore, PELDOR spectroscopy has been used to obtain interactions and distances of radical pairs in disordered samples (Refs. [61,62,130,131]). Recently, this technique has been applied to determine accurately the distance between the two tyrosine radicals in chains A and B of R2 of *E. coli*, giving unequivocal proof that the radical indeed occupies both chains, though with different yields [131]. This technique has a large potential since it does not require crystals. The catalytic reaction of class I RNR involves electron/proton transfer through the interface of R1 and R2 and requires proper docking to a R1–R2 holoenzyme complex, the structure of which is not known in detail. PELDOR experiments on R1–R2 samples (which are in progress, M. Bennati, private communication), with one tyrosyl radical in subunit R2 and one inhibitor radical in subunit R1, or on non-endogenous radical pairs covalently attached to the R1–R2 complex using site-directed spin labeling [132], may open a new way for investigating the structure and function of the active R2–R1 holoenzyme complex.

Acknowledgements

The author thanks his present and previous coworkers and colleagues, G. Bleifuß, M. Galander, M. Kolberg, and S. Pötsch, whose contributions are evident from the references; and in particular, G. Lassmann, for a fruitful cooperation in joint grants on RNR over the past years. M. Bennati is acknowledged for helpful comments on the manuscript. The continuing cooperation with B.-M. Sjöberg, A. Gräslund, M. Högbom, and P. Nordlund, University Stockholm, was the basis for the own work presented in this article. Financial support by Deutsche Forschungsgemeinschaft (DFG La 751/3-1, DFG Le 812/1-2, and DFG Le 812/1-3) is gratefully acknowledged.

References

[1] B.-M. Sjöberg, Ribonucleotide reductases—a group of enzymes with different metallosites and a similar reaction mechanism, Struct. Bond. 88 (1997) 139–173.
[2] B.-M. Sjöberg, The ribonucleotide reductase jigsaw puzzle—a large piece falls into parts, Strucure 2 (1994) 793–796.
[3] J. Stubbe, P. Riggs-Gelasco, Harnessing free radicals: formation and function of the tyrosyl radical in ribonucleotide reductase, Trends Biochem. Sci. 23 (1998) 438–443.
[4] H. Eklund, U. Uhlin, M. Farnegardh, D.T. Logan, P. Nordlund, Structure and function of the radical enzyme ribonucleotide reductase, Prog. Biophys. Mol. Biol. 77 (2001) 177–268.
[5] J. Stubbe, D.G. Nocera, C.S. Yee, M.C.Y. Chang, Radical initiation in the class I ribonucleotide reductase: long-range proton-coupled electron transfer? Chem. Rev. 103 (2003) 2167–2201.
[6] M. Pellegrini, S. Liehr, A.L. Fisher, P.B. Laub, B.S. Cooperman, D.F. Mierke, Structure-based optimization of peptide inhibitors of mammalian ribonucleotide reductase, Biochemistry 39 (2000) 12210–12215.
[7] B.A. Pender, X. Wu, P.H. Axelsen, B.S. Cooperman, Towards a rational design of peptide inhibitors of ribonucleotide reductase: structure–function and modeling studies, J. Med. Chem. 44 (2001) 36–46.
[8] J. Stubbe, J.W.A. van der Donk, Protein radicals in enzyme catalysis, Chem. Rev. 98 (1998) 705–762.
[9] X.Y. Sun, S. Ollagnier, P.P. Schmidt, M. Atta, E. Mulliez, L. Lepape, R. Eliasson, A. Gräslund, M. Fontecave, P. Reichard, B.-M. Sjöberg, The free radical of the anaerobic ribonucleotide reductase from *Escherichia coli* is at glycine 681, J. Biol. Chem. 271 (1996) 6827–6831.
[10] M. Fontecave, E. Mulliez, D.T. Logan, Deoxyribonucleotide synthesis in anaerobic microorganisms: the class III ribonucleotide reductase, Prog. Nucleic Acid Res. 72 (2002) 95–127.
[11] C. Duboc-Toia, A.K. Hassan, E. Mulliez, S. Ollagnier-de Choudens, M. Fontecave, M.C. Leutwein, J. Heider, Very high-field EPR study of glycyl radical enzymes, J. Am. Chem. Soc. 125 (1) (2003) 38–39.
[12] S. Licht, G.J. Gerfen, J.A. Stubbe, Thiyl radicals in ribonucleotide reductases, Science 271 (1996) 477–481.
[13] G.J. Gerfen, S. Licht, J.P. Willems, B.M. Hoffman, J. Stubbe, Electron paramagnetic resonance investigation of a kinetically competent intermediate formed in ribonucleotide reductase: evidence for a thiyl radical-Cob (II) alamin interaction, J. Am. Chem. Soc. 118 (1996) 8192–8197.
[14] M.D. Sintchak, G. Arjara, B.A. Kellogg, J. Stubbe, C.L. Drennan, The crystal structure of class II ribonucleotide reductase reveals how an allosterically regulated monomer mimics a dimer, Nat. Struct. Biol. 9 (2002) 293–300.

[15] D.T. Logan, J. Andersson, B.-M. Sjöberg, P. Nordlund, A glycyl radical site in the crystal structure of a class III ribonucleotide reductase, Science 283 (1999) 1499–1504.
[16] a) P. Nordlund, B.-M. Sjöberg, H. Eklund, Three-dimensional structure of the free radical protein of ribonucleotide reductase, Nature 345 (1990) 593–598;
b) P. Nordlund, H. Eklund, Structure and function of the *Escherichia Coli* ribonucleotide reductase protein R2, J. Mol. Biol. 232 (1) (1993) 123–164.
[17] U. Uhlin, H. Eklund, Structure of ribonucleotide reductase protein R1, Nature 370 (1994) 533–539.
[18] S.S. Mao, T.P. Holler, G.X. Yu , J.M. Bollinger Jr., S. Booker, M.I. Johnston, J. Stubbe, A model for the role of multiple cysteine residues involved in Ribonucleotide reduction—amazing and still confusing, Biochemistry 31 (1992) 9733–9743.
[19] P.E.M. Siegbahn, Theoretical study of the substrate mechanism of ribonucleotide reductase, J. Am. Chem. Soc. 120 (1998) 8417–8429.
[20] P.E.M. Siegbahn, L. Eriksson, F. Himo, M. Pavlov, Hydrogen atom transfer in ribonucleotide reductase (RNR), J. Phys. Chem., B 102 (1998) 10622–10629.
[21] B.M. Sjöberg, M. Sahlin, Thiols in redox mechanism of ribonucleotide reductase, Methods Enzymol. 348 (2002) 1–21.
[22] A. Ehrenberg, Free radical transfer, fluctuating structure and reaction cycle of ribonucleotide reductase, Biosystems 62 (1–3) (2001) 9–12.
[23] A. Ehrenberg, Protein dynamics, free radical transfer and reaction cycle of ribonucleotide reductase, in: H. Frauenfelder, G. Hummer, R. Garcia (Eds.), Biological Physics: third International Symposium, American Institute of Physics, New York, 1999, pp. 163–174.
[24] C.L. Atkin, L. Thelander, P. Reichard, G. Lang, Iron and free-radical in ribonucleotide reductase-exchange of iron and Mossbauer spectroscopy of protein B2 subunit of *Escherichia coli* enzyme, J. Biol. Chem. 248 (21) (1973) 7464–7472.
[25] J.M. Bollinger, W.H. Tong, N. Ravi, B.H. Huynh, D.E. Edmondson, J. Stubbe, Use of rapid kinetics methods to study the assembly of the diferric tyrosyl radical cofactor of *Escherichia coli* ribonucleotide reductase, Methods Enzymol. 258 (1995) 278–303.
[26] W.H. Tong, S. Chen, S.G. Lloyd, D.E. Edmondson, B.H. Huynh, J. Stubbe, Mechanism of assembly of the diferric cluster-tyrosyl radical cofactor of *Escherichia coli* ribonucleotide reductase from the diferrous form of the R2 subunit, J. Am. Chem. Soc. 118 (1996) 2107–2108.
[27] J.P. Willems, H.I. Lee, D. Burdi, P.E. Doan, J. Stubbe, B.M. Hoffman, Identification of the protonated oxygenic ligands of ribonucleotide reductase intermediate X by Q-band H-1,H-2 CW and pulsed ENDOR, J. Am. Chem. Soc. 119 (41) (1997) 9816–9824.
[28] B.E. Sturgeon, D. Burdi, S.X. Chen, B.H. Huynh, D.E. Edmondson, J. Stubbe, B.M. Hoffman, Reconsideration of X, the diiron intermediate formed during cofactor assembly in *E. coli* ribonucleotide reductase, J. Am. Chem. Soc. 118 (32) (1996) 7551–7557.
[29] W.C. Voegtli, N. Khidekel, J. Baldwin, B.A. Ley, J.M. Bollinger, A.C. Rosenzweig, Crystal structure of the ribonucleotide reductase R2 mutant that accumulates a μ-1,2-peroxodiiron(III) intermediate during oxygen activation, J. Am. Chem. Soc. 122 (14) (2000) 3255–3261.
[30] K.K. Andersson, A. Gräslund, Diiron-oxygen proteins, Adv. Inorg. Chem. 43 (1995) 359–408.
[31] A. Gräslund, Ribonucleotide reductase: kinetic methods for demonstrating radical transfer pathway in protein R2 of mouse enzyme in generation of tyrosyl free radical, Methods Enzymol. 354 (2002) 399–414.
[32] M. Sahlin, G. Lassmann, S. Pötsch, B.-M. Sjöberg, A. Gräslund, Transient free radicals in iron/oxygen reconstitution of mutant protein R2 Y122F, J. Biol. Chem. 270 (1995) 12361–12372.
[33] F. Lendzian, M. Sahlin, F. MacMillan, R. Bittl, R. Fiege, S. Pötsch, B.M. Sjöberg, A. Gräslund, W. Lubitz, G. Lassmann, Electronic structure of neutral tryptophane radicals in ribonucleotide reductase studied by EPR and ENDOR spectroscopy, J. Am. Chem. Soc. 118 (34) (1996) 8111–8120.
[34] S. Pötsch, F. Lendzian, R. Ingemarson, A. Hornberg, L. Thelander, W. Lubitz, G. Lassmann, A. Gräslund, The iron-oxygen reconstitution reaction in protein R2 tyr-177 mutants of mouse ribonucleotide reductase-EPR and electron nuclear double resonance studies on a new transient tryptophan radical, J. Biol. Chem. 274 (25) (1999) 17696–17704.
[35] J. Baldwin, C. Krebs, B.A. Ley, D.E. Edmondson, B.H. Huynh, J.H. Bollinger, Mechanism of rapid electron transfer during oxygen activation in the R2 subunit of *Escherichia coli* ribonucleotide reductase. 1. Evidence for a transient tryptophan radical, J. Am. Chem. Soc. 122 (49) (2000) 12195–12206.
[36] C. Krebs, S.X. Chen, J. Baldwin, B.A. Ley, U. Patel, D.E. Edmondson, B.H. Huynh, J.M. Bollinger, Mechanism of rapid electron transfer during oxygen activation in the R2 subunit of *Escherichia coli* ribonucleotide reductase. 2. Evidence for and consequences of blocked electron transfer in the W48F variant, J. Am. Chem. Soc. 122 (49) (2000) 12207–12209.
[37] D. Yun, C. Krebs, G.P. Gupta, D.F. Iwig, B.H. Huynh, J.M. Bollinger, Facile electron transfer during formation of cluster X and kinetic competence of X for tyrosyl radical production in protein R2 of ribonucleotide reductase from mouse, Biochemistry 41 (3) (2002) 981–990.
[38] P.P. Schmidt, U. Rova, B. Katterle, L. Thelander, A. Gräslund, Kinetic evidence that a radical transfer pathway in protein R2 of mouse ribonucleotide reductase is involved in generation of the tyrosyl free radical, J. Biol. Chem. 273 (34) (1998) 21463–21472.
[39] A.L. Persson, M. Sahlin, B.M. Sjöberg, Cysteinyl and substrate radical formation in active site mutant E441Q of *Escherichia coli* class I ribonucleotide reductase, J. Biol. Chem. 273 (47) (1998) 31016–312020.
[40] C.C. Lawrence, M. Bennati, H.V. Obias, G. Bar, R.G. Griffin, J. Stubbe, High-field EPR detection of a disulfide radical anion in the reduction of cytidine 5′diphosphate by the E441Q R1 mutant of *Escherichia coli* ribonucleotide reductase, Proc. Natl. Acad. Sci. U. S. A. 96 (16) (1999) 8979–8984.
[41] K.K. Andersson, P.P. Schmidt, B. Katterle, K.R. Strand, A.E. Palmer, S.K. Lee, E.I. Solomon, A. Gräslund, A.L. Barra, Examples of high-frequency EPR studies in bioinorganic chemistry, J. Biol. Inorg. Chem. 8 (3) (2003) 235–247.
[42] G.J. Gerfen, B.F. Bellew, S. Un, J.M. Bollinger, J. Stubbe, R.G. Griffin, D.J. Singel, High-frequency (139.5 GHz) EPR spectroscopy of the tyrosyl radical in *Escherichia coli* ribonucleotide reductase, J. Am. Chem. Soc. 115 (14) (1993) 6420–6421.
[43] S. Un, M. Atta, M. Fontecave, A.W. Rutherford, *G*-values as a probe of the local protein environment-high-field EPR of tyrosyl radicals in ribonucleotide reductase and photosystem II, J. Am. Chem. Soc. 117 (43) (1995) 10713–10719.
[44] G. Bleifuß, M. Kolberg, S. Pötsch, W. Hofbauer, R. Bittl, W. Lubitz, A. Gräslung, G. Lassmann, F. Lendzian, Tryptophan and tyrosyl radicals in ribonucleotide reductase: a comparative high-field EPR study at 94 GHz, Biochemistry 40 (2001) 15362–15368.
[45] G. Bar, M. Bennati, H.H.T. Nguyen, J. Stubbe, R.G. Griffin, High-frequency (140 GHz) time domain EPR and ENDOR spectroscopy: the tyrosyl radical-diiron cofactor in ribonucleotide reductase from yeast, J. Am. Chem. Soc. 123 (15) (2001) 3569–3576.
[46] K. Möbius, High-field and high-frequency electron paramagnetic resonance, Appl. Magn. Reson. 21 (3–4) (2001) 255.
[47] M. Bennati, J. Stubbe, R.G. Griffin, High-frequency EPR and ENDOR: time-domain spectroscopy of ribonucleotide reductase, Appl. Magn. Res. 21 (3–4) (2001) 389–410.
[48] M. Bennati, C.T. Farrar, J.A. Bryant, S.J. Inati, V. Weis, G.J. Gerfen, P. Riggs-Galesco, J. Stubbe, R.G. Griffin, Pulsed electron-nuclear double resonance (ENDOR) at 140 GHz, J. Magn. Reson. 138 (1999) 232–243.
[49] M. Högbom, M. Galander, M. Andersson, M. Kolberg, W. Hofbauer,

G. Lassmann, P. Nordlund, F. Lendzian, Displacement of the tyrosyl radical cofactor in ribonucleotide reductase obtained by single-crystal high-field EPR and 1.4-angstrom X-ray data, Proc. Natl. Acad. Sci. U. S. A. 100 (6) (2003) 3209–3214.

[50] W. Lubitz, F. Lendzian, ENDOR Spectroscopy, Advances in Photosynthesis. "Biophysical Techniques in Photosynthesis", Kluwer, Dordrecht, 1996, pp. 255–275.

[51] C.W. Hoganson, M. Sahlin, B.M. Sjöberg, G.T. Babcock, Electron magnetic resonance of the tyrosyl radical in ribonucleotide reductase from *Escherichia coli*, J. Am. Chem. Soc. 118 (1996) 4672–4679.

[52] C.J. Bender, M. Sahlin, G.T. Babcock, B.A. Barry, T.K. Chandrashekar, S.P. Salowe, J. Stubbe, B. Lindstrom, L. Petersson, A. Ehrenberg, B.M. Sjöberg, An ENDOR study of the tyrosyl free radical in ribonucleotide reductase from *Escherichia coli*, J. Am. Chem. Soc. 111 (21) (1989) 8076–8083.

[53] A. Mezzetti, A.L. Maniero, M. Brustolon, G. Giacometti, L.C. Brunel, A tyrosyl radical in an irradiated single crystal of *N*-acetyl-L-tyrosine studied by X-band cw-EPR, high-frequency EPR, and ENDOR spectroscopies, J. Phys. Chem. A 103 (48) (1999) 9636–9643.

[54] A. Carrington, A.D. McLachlan, Introduction to Magnetic Resonance, Harper & Row, New York, 1969, pp. 137–138.

[55] J.A. Weil, J.R. Bolton, J.E. Wertz, Electron Paramagnetic Resonance, Wiley, New York, 1994, pp. 239–276.

[56] J.E. Huyett, P.E. Doan, R. Gurbiel, A.L.P. Houseman, M. Sivaraja, D.B. Goodin, B.M. Hoffman, Compound ES of cytochrome-*C* peroxidase contains a Trp π-cation radical-characterization by cw and pulsed Q-band ENDOR spectroscopy, J. Am. Chem. Soc. 117 (35) (1995) 9033–9041.

[57] N.M. Atherton, Principles of Magnetic Resonance, Ellis Horwood, New York, 1993, pp. 169–223.

[58] A. Schweiger, Pulsed electron-spin-resonance spectroscopy—basic principles, techniques, and examples of applications, Angew. Chem., Int. Ed. 30 (3) (1991) 265–292.

[59] T. Prisner, M. Rohrer, F. MacMillan, Pulsed EPR spectroscopy: biological applications, Annu. Rev. Phys. Chem. 52 (2001) 279–313.

[60] B.M. Hoffman, Electron-nuclear double resonance spectroscopy (and electron spin-echo envelope modulation spectroscopy) in bioinorganic chemistry, Proc. Natl. Acad. Sci. 100 (2003) 3575–3578.

[61] A. Schweiger, G. Jeschke, Principles of Pulse Electron Paramagnetic Resonance, Oxford Univ. Press, Oxford, 2001.

[62] G. Jeschke, Distance measurements in the nanometer range by pulse EPR, Chem Phys Chem 3 (2002) 927–932.

[63] A. Ehrenberg, P. Reichard, Electron-spin resonance of iron-containing protein B2 from ribonucleotide reductase, J. Biol. Chem. 247 (11) (1972) 3485–3488.

[64] B.M. Sjöberg, P. Reichard, A. Gräslund, A. Ehrenberg, Nature of free-radical in ribonucleotide reductase from *Escherichia coli*, J. Biol. Chem. 252 (2) (1977) 536–541.

[65] P.J. van Dam, J.P. Willems, P.P. Schmidt, S. Pötsch, A.-L. Barra, W.R. Hagen, B.M. Hoffman, K.K. Andersson, A. Gräslund, High-frequency EPR and pulsed Q-Band ENDOR studies on the origin of the hydrogen bond in tyrosyl radicals of ribonucleotide reductase R2 proteins from mouse and herpes simplex virus type 1, J. Am. Chem. Soc. 120 (20) (1998) 5080–5085.

[66] A. Chabes, V. Domkin, G. Larsson, A.M. Liu, A. Gräslund, S. Wijmenga, L. Thelander, Yeast ribonucleotide reductase has a heterodimeric iron-radical-containing subunit, Proc. Natl. Acad. Sci. U. S. A. 97 (2000) 2474–2479.

[67] W.C. Voegtli, J. Ge, D.L. Perlstein, J. Stubbe, A.C. Rosenzweig, Structure of the yeast ribonucleotide reductase Y2Y4 heterodimer, Proc. Natl. Acad. Sci. U. S. A. 98 (2001) 10073–10078.

[68] M. Fontecave, C. Gerez, Tyrosyl radicals and ribonucleotide reductase, Methods Enzymol. 348 (2002) 21–30.

[69] S. Sauge-Merle, P.L. Laulhere, J. Coves, L. le Pape, S. Menage, M. Fontecave, Ribonucleotide reductase from the higher plant *Arabidopsis thaliana*: expression of the R2 component and characterization of its iron-radical center, J. Biol. Inorg. Chem. 2 (1997) 586–594.

[70] A.M. Liu, A.L. Barra, H. Rubin, G.Z. Lu, A. Gräslund, Heterogeneity of the local electrostatic environment of the tyrosyl radical in *Mycobacterium tuberculosis* ribonucleotide reductase observed by high-field electron paramagnetic resonance, J. Am. Chem. Soc. 122 (9) (2000) 1974–1978.

[71] P.P. Schmidt, K.K. Andersson, A.L. Barra, L. Thelander, A. Gräslund, High field EPR studies of mouse ribonucleotide reductase indicate hydrogen bonding of the tyrosyl radical, J. Biol. Chem. 271 (39) (1996) 23518–23615.

[72] A. Liu, S. Pötsch, A. Davidov, A.L. Barra, H. Rubin, A. Gräslund, The tyrosyl free radical of recombinant ribonucleotide reductase from *Mycobacterium tuberculosis* is located in a rigid hydrophobic pocket, Biochemistry 37 (46) (1998) 16369–16377.

[73] P. Allard, A.L. Barra, K.K. Andersson, P.P. Schmidt, M. Atta, A. Gräslund, Characterization of a new tyrosyl free radical in *Salmonella typhimurium* ribonucleotide reductase with EPR at 9.45 and 245 GHz, J. Am. Chem. Soc. 118 (4) (1996) 895–896.

[74] Y. Huque, F. Fieschi, E. Torrents, I. Gibert, R. Eliasson, P. Reichard, M. Sahlin, B.M. Sjöberg, The active form of the R2F protein of class Ib ribonucleotide reductase from *Corynebacterium ammoniagenes* is a diferric protein, J. Biol. Chem. 275 (33) (2000) 25365–25371.

[75] M. Högbom, Y. Huque, B.M. Sjöberg, P. Nordlund, Crystal structure of the diiron/radical protein of ribonucleotide reductase from *Corynebacterium ammoniagenes*, Biochemistry 41 (4) (2002) 12381–12389.

[76] M. Eriksson, A. Jordan, H. Eklund, Structure of *Salmonella typhimurium* nrdF ribonucleotide reductase in its oxidized and reduced forms, Biochemistry 37 (38) (1998) 13359–13369.

[77] R. Eliasson, E. Pontis, A. Jordan, P. Reichard, Allosteric regulation of the third ribonucleotide reductase(NrdEF enzyme) from enterobacteriaceae, J. Biol. Chem. 2271 (1996) 26582–26587.

[78] F. Himo, A. Gräslund, L.A. Eriksson, Density functional calculations on model tyrosyl radicals, Biophys. J. 72 (4) (1997) 1556–1567.

[79] K. Warncke, M.S. Perry, Redox state dependence of rotamer distributions in tyrosine and neutral tyrosyl radical, BBA-Protein Struct. M 1545 (1–2) (2001) 1–5.

[80] C.W. Hoganson, G.T. Babcock, Protein-tyrosyl radical interactions in photosystem II studied by electron spin resonance and electron nuclear double resonance spectroscopy: comparison with ribonucleotide reductase and in vitro tyrosine, Biochemistry 31 (1992) 11874–11880.

[81] A.J. Stone, G-factors of aromatic free radicals, Mol. Phys. 6 (5) (1963) 509–515.

[82] S. Un, C. Gerez, E. Elleingand, M. Fontecave, Sensitivity of tyrosyl radical *g*-values to changes in protein structure: a high-field EPR study of mutants of ribonucleotide reductase, J. Am. Chem. Soc. 123 (2001) 3048–3054.

[83] G. Bleifuß, S. Pötsch, W. Hofbauer, A. Gräslund, W. Lubitz, G. Lassmann, F. Lendzian, High-field EPR at 94 GHz of amino acid radicals in ribonucleotide reductase, magnetic Resonance and related Phenomena, vol. II, Proceedings of the Joint 29th AMPERE-13thISMAR Conference, 1998, pp. 879–880, Technische Universität Berlin, ISBN 3-7983-1780-1.

[84] M. Engström, F. Himo, A. Gräslund, B. Minaev, O. Vahtras, H. Agren, Hydrogen bonding to tyrosyl radical analyzed by ab initio *g*-tensor calculations, J. Phys. Chem., A 104 (21) (2000) 5149–5153.

[85] H. Tanaka, H. Arakawa, T. Yamaguchi, K. Shiraishi, S. Fukuda, K. Matsui, Y. Takei, Y. Nakamura, A ribonucleotide reductase gene involved in a p53-dependent cell-cycle checkpoint for DNA damage, Nature 404 (6773) (2000) 42–49.

[86] O. Guittet, P. Hakansson, N. Voevodskaya, S. Fridd, A. Gräslund, H. Arakawa, Y. Nakamura, L. Thelander, Mammalian p53R2 protein forms an active ribonucleotide reductase in vitro with the R1 protein, which is expressed both in resting cells in response to DNA

damage and in proliferating cells, J. Biol. Chem. 276 (44) (2001) 40647–40651.
[87] C. Aubert, P. Mathis, A.P.M. Eker, K. Brettel, Intraprotein electron transfer between tyrosine and tryptophan in DNA photolyase from *Anacystis nidulans*, Proc. Natl. Acad. Sci. U. S. A. 96 (10) (1999) 5423–5427.
[88] S. Weber, C.W.M. Kay, H. Mögling, K. Möbius, K. Hitomi, T. Todo, Photoactivation of the flavin cofactor in *Xenopus laevis* photolyase: observation of a transient tyrosyl radical by time-resolved electron paramagnetic resonance, Proc. Natl. Acad. Sci. U. S. A. 99 (2002) 1319–1322.
[89] C. Aubert, M.H. Vos, P. Mathis, A.P.M. Eker, K. Brettel, Intraprotein radical transfer during photoactivation of DNA photolyase, Nature 405 (2000) 586–590.
[90] A. Ivancich, C. Jakopitsch, M. Auer, S. Un, C. Obinger, Protein-based radicals in the catalase-peroxidase of *Synechocystis* PCC6803: a multifrequency EPR investigation of wild-type and variants on the environment of the heme active site, J. Am. Chem. Soc. 125 (2003) 14093–14102.
[91] B. Katterle, M. Sahlin, P.P. Schmidt, S. Pötsch, D.T. Logan, A. Gräslund, B.M. Sjöberg, Kinetics of transient radicals in *Escherichia coli* ribonucleotide reductase—formation of a new tyrosyl radical in mutant protein R2, J. Biol. Chem. 272 (16) (1997) 10414–10421.
[92] B. Kauppi, B.B. Nielsen, S. Ramaswamy, I. Kjoller-Larsen, M. Thelander, H. Eklund, The three-dimensional structure of mammalian ribonucleotide reductase protein R2 reveals a more-accessible iron-radical site than *Escherichia coli* R2, J. Mol. Biol. 262 (1996) 706–720.
[93] A. Adrait, M. Öhrström, A.L. Barra, L. Thelander, A. Gräslund, EPR studies on a stable sulfinyl radical observed in the iron-oxygen-reconstituted Y177F/I263C protein R2 double mutant of ribonucleotide reductase from mouse, Biochemistry 41 (20) (2002) 6510–6516.
[94] E.I. Solomon, T.C. Brunold, M.I. Davis, J.N. Kemsley, S.-K. Lee, N. Lehnert, F. Neese, A.J. Skulan, Y.-S. Yang, J. Zhou, Geometric and electronic structure/function correlations in non-heme iron enzymes, Chem. Rev. 100 (1) (2000) 235–349.
[95] B.J. Wallar, J.D. Lipscomb, Dioxygen activation by enzymes containing binuclear non-heme iron clusters, Chem. Rev. 96 (7) (1996) 2625–2657.
[96] A.C. Rosenzweig, H. Brandstetter, D.A. Whittington, P. Nordlund, S.J. Lippard, C.A. Frederick, Crystal structures of the methane monooxygenase hydroxylase from *Methylococcus capsulatus* (Bath): implications for substrate gating and component interactions, Proteins 29 (2) (1997) 141–152.
[97] M.-H. Baik, M. Newcomb, R.A. Friesner, S.J. Lippard, Mechanistic Studies on the Hydroxylation of Methane by Methane Monooxygenase, Chem. Rev. 103 (2003) 2385–2419.
[98] D.T. Logan, F. DeMare, B.O. Persson, A. Slaby, B.-M. Sjöberg, P. Nordlund, Crystal structures of two self-hydroxylating ribonucleotide reductase protein R2 mutants: structural basis for the oxygen-insertion step of hydroxylation reactions catalyzed by diiron proteins, Biochemistry 37 (1998) 10798–10807.
[99] J. Baldwin, W.C. Voegtli, N. Khidekel, P. Moenne-Lopez, C. Krebs, A.S. Pereirra, B.A. Ley, B.H. Huynh, T.M. Loehr, P.J. Riggs-Gelasco, A.C. Rosenzweig, J.M. Bollinger, Rational reprogramming of the R2 subunit of *Escherichia coli* ribonucleotide reductase into a self-hydroxylating monooxygenase, J. Am. Chem. Soc. 123 (2001) 7017–7030.
[100] M. Assarsson, M.E. Andersson, M. Högbom, B.O. Persson, M. Sahlin, A.L. Barra, B.M. Sjöberg, P. Nordlund, A. Gräslund, Restoring proper radical generation by azide binding to the iron site of the E238A mutant R2 protein of ribonucleotide reductase from *Escherichia coli*, J. Biol. Chem. 276 (29) (2001) 26852–26859.
[101] A. Liu, M. Sahlin, S. Pötsch, B.M. Sjöberg, A. Gräslund, New paramagnetic species formed at the expense of the transient tyrosyl radical in mutant protein R2 F208Y of *Escherichia coli* ribonucleotide reductase, Biochem. Biophys. Res. Commun. 246 (3) (1998) 740–745.
[102] M. Kolberg, G. Bleifuß, S. Pötsch, A. Gräslund, W. Lubitz, G. Lassmann, F. Lendzian, A new stable high-valent diiron center in R2 mutant Y122H of *E. coli* ribonucleotide reductase studied by high-field EPR and Fe-57-ENDOR, J. Am. Chem. Soc. 122 (40) (2000) 9856–9857.
[103] H. Thomann, M. Bernardo, J.M. McCormick, S. Pulver, K.K. Andersson, J.D. Lipscomb, E.I. Solomon, Pulsed EPR studies of mixed valent [Fe(II)Fe(III)] forms of hemerythrin and methane monooxygenase: evidence for a hydroxide bridge, J. Am. Chem. Soc. 115 (1993) 8881–8882.
[104] F. Lendzian, M. Kolberg, G. Bleifuss, G. Lassmann, A. Gräslund, W. Lubitz, A strongly coupled diiron/radical state in ribonucleotide reductase mutant Y122H of *E. coli* studied by Fe-57- and H-1/H-2-ENDOR, J. Inorg. Biochem. 86 (1) (2001) 314.
[105] M.E. Andersson, M. Högbom, A. Rinaldo-Matthis, K.K. Andersson, B.M. Sjöberg, P. Nordlund, The crystal structure of an azide complex of the diferrous R2 subunit of ribonucleotide reductase displays a novel carboxylate shift with important mechanistic implications for diiron-catalyzed oxygen activation, J. Am. Chem. Soc. 121 (11) (1999) 2346–2352.
[106] N. Ravi, J.M. Bollinger, B.H. Huynh, D.E. Edmondson, J. Stubbe, Mechanism of assembly of the tyrosyl radical-diiron(III) cofactor of *Escherichia coli*, J. Am. Chem. Soc. 116 (18) (1994) 8007–8014.
[107] M. Kolberg, Generation and characterization of free and metal-associated amino acid radicals in ribonucleotide reductase using EPR techniques, PhD thesis, Technical University Berlin, Germany, 2001.
[108] M.D. Snodin, L. Ould-Moussa, U. Wallmann, S. Lecomte, V. Bachler, E. Bill, H. Hummel, T. Weyhermüller, P. Hildebrandt, K. Wieghardt, Complexes and their phenoxyl radical analogues: a Mössbauer and resonance Raman spectroscopic study, Chem. Eur. J. 5 (1999) 2554–2565.
[109] J.W. Whittaker, Free radical catalysis by galactose oxidase, Chem. Rev. 103 (2003) 2347–2363.
[110] M. Kaupp, T. Gress, R. Reviakine, O.L. Malkina, V.G. Malkin, g tensor and spin density of the modified tyrosyl radical in galactose oxidase: a density functional study, J. Phys. Chem., B 107 (2003) 331–337.
[111] D.T. Logan, X.D. Su, A. Aberg, K. Regnström, J. Hajdu, H. Eklund, P. Nordlund, Crystal structure of reduced protein R2 of ribonucleotide reductase: the structural basis for oxygen activation at a dinuclear iron site, Structure 4 (9) (1996) 1053–1064.
[112] M. Sahlin, B.M. Sjöberg, G. Backes, T. Loehr, J. Sanders-Loehr, Activation of the iron-containing B2-protein of ribonucleotide reductase by hydrogen-peroxide, Biochem. Biophys. Res. Commun. 167 (2) (1990) 813–818.
[113] M.A. Miller, F.T. Gobena, K. Kauffmann, E. Munck, L. Que, M.T. Stankovich, Differing roles for the diiron clusters of ribonucleotide reductase from aerobically crown *Escherichia coli* in the generation of the Y122 radical, J. Am. Chem. Soc. 121 (5) (1999) 1096–1097.
[114] B.M. Sjöberg, A. Gräslund, F. Eckstein, A substrate radical intermediate in the reaction between ribonucleotide reductase from *Escherichia coli* and 2′-azido-2′-deoxynucleoside diphosphates, J. Biol. Chem. 258 (13) (1983) 8060–8067.
[115] W.A. van der Donk, J. Stubbe, G.J. Gerfen, B.F. Bellew, R.G.Griffin, EPR investigations of the inactivation of *Escherichia coli* ribonucleotide reductase with 2′-azido-2′-deoxyuridine 5′-diphosphate-Evidence for the involvement of the thiyl radical of C225-R1, J. Am. Chem. Soc. 117 (35) (1995) 8908–8916.
[116] G.J. Gerfen, W.A. van der Donk, G.X. Yu, J.R. McCarthy, E.T. Jarvi, D.P. Matthews, C. Farrar, R.G. Griffin, J. Stubbe, Characterization of a substrate-derived radical detected during the inactivation of ribonucleotide reductase from *Escherichia coli* by 2′-fluoromethylene-2′-deoxycytidine 5′-diphosphate, J. Am. Chem. Soc. 120 (16) (1998) 3823–3835.

[117] J.A. Stubbe, W.A. van der Donk, Ribonucleotide reductases: radical enzymes with suicidal tendencies, Chem. Biol. 2 (12) (1995) 793–801.
[118] W.A. van der Donk, G.X. Yu, L. Perez, R.J. Sanchez, J. Stubbe, V. Samano, M.J. Robins, Detection of a new substrate-derived radical during inactivation of ribonucleotide reductase from *Escherichia coli* by gemcitabine 5′diphosphate, Biochemistry 37 (18) (1998) 6419–6426.
[119] L. Thelander, B. Larsson, Active-site of ribonucleoside diphosphate reductase from *Escherichia coli*—inactivation of enzyme by 2′substituted ribonucleoside diphosphates, J. Biol. Chem. 251 (5) (1976) 1398–1405.
[120] J. Coves, L.L.H. de Fallois, L. le Pape, J.L. Decout, M. Fontecave, Inactivation of *Escherichia coli* ribonucleotide reductase by 2′deoxy-2′mercaptouridine 5′diphosphate. Electron paramagnetic resonance evidence for a transient protein perthiyl radical, Biochemistry 35 (26) (1996) 8595–8602.
[121] D.J. Nelson, R.L. Petersen, M.C.R. Symons, Unstable intermediates. 178. Structure of intermediates formed in radiolysis of thiols, J. Chem. Soc., Perkins Trans. 2 (15) (1977) 2005–2015.
[122] K. Matsuki, J.H. Hadley, W.H. Nelson, C. Yang, ESR studies of monosulfide radicals in irradiated *N*-acetyl-L-cysteine single crystals, J. Magn. Reson. 103 (1993) 196–202.
[123] M. Kolberg, G. Bleifuss, A. Gräslund, B.M. Sjöberg, W. Lubitz, F. Lendzian, G. Lassmann, Protein thiyl radicals directly observed by EPR spectroscopy, Arch. Biochem. Biophys. 403 (2002) 141–144.
[124] M. van Gastel, W. Lubitz, G. Lassmann, F. Neese, Electronic Structure of the Cysteine Thiyl Radical: A DFT and Correlated ab Initio Study, J. Am. Chem. Soc. 126 (2004) 2237–2246.
[125] M. Kolberg, G. Bleifuss, B.M. Sjöberg, A. Gräslund, W. Lubitz, F. Lendzian, G. Lassmann, Generation and electron paramagnetic resonance spin trapping detection of thiyl radicals in model proteins and in the R1 subunit of *Escherichia coli* ribonucleotide reductase, Arch. Biochem. Biophys. 397 (2002) 57–68.
[126] A.L. Persson, M. Eriksson, B. Katterle, S. Pötsch, M. Sahlin, B.M. Sjöberg, A new mechanism-based radical intermediate in a mutant R1 protein affecting the catalytically essential Glu(441) in *Escherichia coli* ribonucleotide reductase, J. Biol. Chem. 272 (50) (1997) 31533–31541.
[127] D. Becker, S. Swarts, M. Champagne, M.D. Sevila, An electron-spin-resonance investigation of the reactions of glutathione: cysteine and penicillamine thiyl radicals-competitive formation of $RSO^{\bullet}$, $RSSR^{-}$, and RSS, Int. J. Radiat. Biol. 53 (5) (1988) 767–786.
[128] J.H. Hadley, W. Gordy, Coupling of S-33 and nature of free radicals in irradiated crystals of cystine dihydrochloride: 2. Charged radicals, Proc. Natl. Acad. Sci. U. S. A. 71 (11) (1974) 4409–4413.
[129] F. Himo, P.E.M. Siegbahn, Very stable ribonucleotide substrate radical relevant for class I ribonucleotide reductase, J. Phys. Chem., B 104 (31) (2000) 7502–7509.
[130] C. Elsässer, M. Brecht, R. Bittl, Pulsed electron–electron double resonance on multinuclear metal clusters: assignment of spin projection factors based on the dipolar interaction, J. Am. Chem. Soc. 124 (42) (2002) 12606–12611.
[131] M. Bennati, A. Weber, J. Antonic, D.L. Perlstein, J. Robblee, J. Stubbe, Pulsed ELDOR spectroscopy measures the distance between the two tyrosyl radicals in the R2 subunit of the *E. coli* ribonucleotide reductase, J. Am. Chem. Soc. 125 (2003) 14988–14989.
[132] H.J. Steinhoff, B. Suess, Molecular mechanisms of gene regulation studied by site-directed spin labeling, Methods 29 (2) (2003) 188–195.